Manuscript prepared for Atmos. Chem. Phys. Discuss.
with version 2014/05/30 6.91 Copernicus papers of the LaTeX class copernicus.cls.
Date: 31 December 2014

WRF-chem model predictions of the regional impacts of N_2O_5 heterogeneous processes on nighttime chemistry over north-western Europe

D. Lowe[1], S. Archer-Nicholls[1], W. Morgan[1], J. Allan[1,2], S. Utembe[3], B. Ouyang[4], E. Aruffo[5], M. Le Breton[1], R. A. Zaveri[6], P. Di Carlo[5], C. Percival[1], H. Coe[1], R. Jones[4], and G. McFiggans[1]

[1]School of Earth, Atmospheric & Environmental Sciences, University of Manchester, Manchester, UK
[2]National Centre for Atmospheric Science, University of Manchester, Manchester, UK
[3]School of Earth Sciences, University of Melbourne, Victoria 3010, Australia
[4]Department of Chemistry, University of Cambridge, Cambridge, UK
[5]CETEMPS – Dipartimento di Fisica, Universita di L'Aquila, L'Aquila, Italy
[6]Atmospheric Sciences and Global Change Division, Pacific Northwest National Laboratory, Richland, Washington, USA

Correspondence to: G. McFiggans (g.mcfiggans@manchester.ac.uk)

Abstract

Chemical modelling studies have been conducted over north-western Europe in summer conditions, showing that night-time dinitrogen pentoxide (N_2O_5) heterogeneous reactive uptake is important regionally in modulating particulate nitrate and has a modest influence on oxidative chemistry. Results from WRF-Chem model simulations, run with a detailed volatile organic compound (VOC) gas-phase chemistry scheme and the MOSAIC sectional aerosol scheme, were compared with a series of airborne gas and particulate measurements made over the UK in July 2010. Modelled mixing ratios of key gas-phase species were reasonably accurate (correlations with measurements of 0.7–0.9 for NO_2 and O_3). However modelled loadings of particulate species were less accurate (correlation with measurements for particulate sulphate and ammonium were between 0.0–0.6). Sulphate mass loadings were particularly low (modelled means of 0.5–0.7 $\mu g\, kg_{air}^{-1}$, compared with measurements of 1.0–1.5 $\mu g\, kg_{air}^{-1}$). Two flights from the campaign were used as testcases – one with low relative humidity (RH) (60–70 %), the other with high RH (80–90 %). N_2O_5 heterogeneous chemistry was found to not important in the low RH testcase; but in the high RH testcase it had a strong effect, and significantly improved the agreement between modelled and measured NO_3 and N_2O_5. When the model failed to capture atmospheric RH correctly, the modelled NO_3 and N_2O_5 mixing ratios for these flights differed significantly from the measurements. This demonstrates that, for regional modelling which involves heterogeneous processes, it is essential to capture the ambient temperature and water vapour profiles.

The night-time NO_3 oxidation of VOCs across the whole region was found to be $\times$ 100–300 slower than the daytime OH oxidation of these compounds. The difference in contribution was less for alkenes ($\times$ 80), and comparable for DMS. However the suppression of NO_3 mixing ratios across the domain by N_2O_5 heterogeneous chemistry has only a very slight, negative, influence on this oxidative capacity. The influence on regional particulate nitrate mass loadings is stronger. Night-time N_2O_5 heterogeneous chemistry maintains the production of particulate nitrate within polluted regions: when this process is taken into consideration, the daytime peak (for the 95th percentile) of PM_{10} nitrate mass loadings remains around 5.6 $\mu g\, kg_{air}^{-1}$, but the

nighttime minimum increases from 3.5 to 4.6 $\mu g\,kg_{air}^{-1}$. The sustaining of higher particulate mass loadings through the night by this process improves model skill at matching measured aerosol nitrate diurnal cycles, and will negatively impact on regional air quality, requiring this process to be included in regional models.

1 Introduction

The hydroxyl radical (OH) dominates the oxidative control of the composition of the troposphere, primarily through its established role as a daytime oxidant. However, night time chemistry, driven primarily by the nitrate radical (NO_3), has been increasingly recognised over the last decade as also being atmospherically important (cf. Brown and Stutz, 2012). NO_3 plays a key role in controlling the atmospheric burden of nonmethane volatile organic compounds (NMVOCs) (cf. Atkinson and Arey, 2003), sulphur containing compounds such as dimethylsulfide (DMS) (Winer et al., 1984; Platt and Le Bras, 1997), and the aerosol burden, through indirect production of aerosol nitrate (NO_3^-) (Heikes and Thompson, 1983; Li et al., 1993) and creation of less volatile oxidised organic compounds which can condense and add to secondary organic aerosol (SOA) mass (cf. Hoyle et al., 2011).

In polluted environments, the formation of NO_3 is rapid, but its sinks are abundant, and so its turnover is very fast. The primary source of NO_3 in the troposphere is through the reaction:

$$O_3 + NO_2 \rightarrow NO_3 + O_2, \tag{R1}$$

During the daytime, NO_3 is quickly photolysed back to NO_x, with a lifetime of around 5 s (Atkinson, 2000). It also readily reacts with NO to form NO_2 (Asaf et al., 2010):

$$NO_3 + NO \rightarrow 2NO_2. \tag{R2}$$

However, at night photolysis is insignificant and concentrations of NO are small away from local sources, as it is no longer produced from photolysis of NO_2 and is quickly titrated by O_3. This allows concentrations of NO_3 to build up, particularly higher up in the lower troposphere where there is more O_3 and significant levels of NO_2 (Allan et al., 2000). Night-time

concentrations of NO_3 are typically a few tens of pptv, although peak levels of over 800 pptv have been reported (Asaf et al., 2010). NO_3, once produced, further reacts with NO_2 to produce dinitrogen pentoxide (N_2O_5), which can act as as a reactive reservoir species for NO_3:

$$NO_3 + NO_2 \overset{M}{\rightleftharpoons} N_2O_5. \tag{R3}$$

This is readily reversible, as N_2O_5 is thermally unstable and NO_3 and N_2O_5 quickly establish an equilibrium:

$$[N_2O_5] = K_{eq}[NO_2][NO_3], \tag{1}$$

where K_{eq} is a temperature dependent equilibrium constant (Chang et al., 2011). With cooler temperatures, as found at high altitudes and at night, and/or in polluted regions with higher levels of NO_2, $[N_2O_5]$ may be much greater than $[NO_3]$ (Osthoff et al., 2007).

NO_3 is directly lost via gas-phase reactions with DMS and NMVOCs. The reaction with DMS proceeds through the abstraction of a hydrogen atom, forming nitric acid and the CH_3SCH_2 radical (Butkovskaya and LeBras, 1994):

$$NO_3 + CH_3SCH_3 \rightarrow HNO_3 + CH_3SCH_2. \tag{R4}$$

CH_3SCH_2 reacts with O_2 to form the $CH_3SCH_2O_2$ peroxy-radical, which reacts further to form CH_3S and formaldehyde. Although Reaction (R4) is the rate-limiting step in this chain, it still occurs fast enough ($1.1 \times 10^{-12}\,cm^3\,molecule^{-1}\,s^{-1}$ at 298 K; Atkinson et al., 2004) for it to be important in the marine sulpher cycle (CH_3S reacts further to eventually form either SO_2 or H_2SO_4; cf. von Glasow and Crutzen, 2004). Reactions of NO_3 with saturated hydrocarbons proceed via hydrogen abstraction, forming nitric acid and an alkyl radical; however these are relatively slow (with rate constants typically smaller than $3 \times 10^{-16}\,cm^3\,molecule^{-1}\,s^{-1}$; cf. Atkinson and Arey, 2003) and so unimportant compared with OH driven reactions. Reactions of NO_3 with alkenes proceed via addition to the carbon double bond and are faster, particularly for larger ($C > 3$) biogenic alkenes (such as isoprene, and the various terpenes), making these

reactions more important for hydrocarbon budgets (cf. Brown and Stutz, 2012). For example, isoprene reacts with NO_3 at the rate $7 \times 10^{-13}\,cm^3\,molecule^{-1}\,s^{-1}$:

$$NO_3 + CH_2{=}C(CH_3)CH{=}CH_2 \rightarrow CH_2(ONO_2)C(CH_3)CH{=}CH_2. \quad \text{(R5)}$$

The resultant nitroxyalkyl radicals can then thermally decompose, but most react quickly with O_2 to form nitroxyalkyl-peroxy radicals (RO_2) which can go on to react with NO_2, NO_3, HO_2, or other peroxy radicals. The relative importance of the different reaction channels for RO_2 in the real atmosphere is currently unclear, while $RO_2 + HO_2$ appears to not be significant, modelling studies are ambiguous (and laboratory studies too limited) as to which of $RO_2 + NO_3$ and $RO_2 + RO_2$ are more important (cf. Brown and Stutz, 2012, and references therein).

In addition to the direct losses of NO_3, there are several loss mechanisms for N_2O_5 in the atmosphere, as described in more detail by Chang et al. (2011). Gas phase N_2O_5 hydrolysis:

$$N_2O_{5\,(g)} + H_2O_{(g)} \rightarrow 2HNO_{3\,(g)}, \quad \text{(R6)}$$

proceeds too slowly to have a significant impact on the concentrations of NO_3 and N_2O_5 (Dentener and Crutzen, 1993). Heterogeneous uptake of N_2O_5 to aerosol particles or cloud droplets is a more important loss. As NO_3 and N_2O_5 are in chemical equilibrium, this direct loss of N_2O_5 is an indirect and sometimes dominant loss mechanisms for NO_3. Heterogeneous hydrolysis of N_2O_5 is the thought to be the dominant pathway (Dentener and Crutzen, 1993), occurring through the reaction:

$$N_2O_{5\,(g)} + H_2O_{(l)} \rightarrow 2HNO_{3\,(aq)}, \quad \text{(R7)}$$

where the HNO_3 produced from heterogeneous hydrolysis contributes to the nitrate aerosol burden in the atmosphere.

N_2O_5 also readily reacts with halide ions in the condensed phase summarised as follows in Bertram and Thornton (2009):

$$N_2O_{5\,(g)} + X^-_{(aq)} \rightarrow XNO_{2\,(g)} + NO^-_{3\,(aq)}, \quad \text{(R8)}$$

where X^- is the halide ion (chloride Cl^- or bromide Br^-). Where X^- is Cl^-, this process is a proposed source of nitryl chloride $ClNO_2$ in the gas phase, although measurements in the marine boundary layer and continental air show higher concentrations than would be predicted through this mechanism, suggesting further mechanisms for production or that our current understanding underestimates the impact of this process (Thornton et al., 2010).

The rate of the heterogeneous reaction can be reduced to a simple first-order process:

$$\left.\frac{\mathrm{d}[N_2O_5]}{\mathrm{d}t}\right|_{\mathrm{het}} = -k_{N_2O_5}[N_2O_5], \tag{2}$$

where $k_{N_2O_5}$ is the mass-transfer coefficient for N_2O_5:

$$k_{N_2O_5} = 4\pi\overline{R_\mathrm{p}}D_{\mathrm{g},N_2O_5}N_\mathrm{p}f(Kn_{N_2O_5},\alpha_{N_2O_5}), \tag{3}$$

where $\overline{R_\mathrm{p}}$ is the mean aerosol particle radius, D_{g,N_2O_5} is the gas diffusivity of N_2O_5, N_p is the aerosol particle number and $f(Kn_{N_2O_5},\gamma_{N_2O_5})$ is the transition regime correction factor, dependent on the Knudsen number ($Kn_{N_2O_5}$) and a mass accommodation coefficient characterising the interfacial mass transport limitation ($\alpha_{N_2O_5}$). The uptake of N_2O_5 is dependent on its reactivity with the compounds in the aerosol particle, and so can we replace $\alpha_{N_2O_5}$ with its reaction probability $\gamma_{N_2O_5}$ instead. $\gamma_{N_2O_5}$ is strongly dependent on aerosol composition and water content, being greatest on aqueous solutions of ammonium sulphate or sodium sulphate (for which $\gamma_{N_2O_5}$ approaches 0.03), and lowest on solid particles, or organic or nitrate containing solutions (which can reduce $\gamma_{N_2O_5}$ by a factor of 10 or more, see Chang et al., 2011, and references therein).

There have been several parameterisations developed for N_2O_5 chemistry over recent years (e.g. Davis et al., 2008; Bertram and Thornton, 2009). The parameterisation of Bertram and Thornton (2009) accommodates both (R7) and (R8) into a single expression for $\gamma_{N_2O_5}$:

$$\gamma_{N_2O_5} = Ak'_{2f}\left(1 - \frac{1}{\left(\frac{k_3[H_2O_{(l)}]}{k_{2b}[NO_3^-]}\right) + 1 + \left(\frac{k_4[Cl^-]}{k_{2b}[NO_3^-]}\right)}\right), \tag{4}$$

where $A = 3.2 \times 10^{-8} s$ is an empirical pre-factor, its derivation described in full detail by Bertram and Thornton (2009). k'_{2f} is defined as:

$$k'_{2f} = \beta - \beta e^{(-\delta[\mathrm{H_2O_{(l)}}])}, \quad (5)$$

with the experimentally determined $\beta = 1.15 \times 10^6\,\mathrm{s^{-1}}$ and $\delta = 1.3 \times 10^{-1}\,\mathrm{M^{-1}}$. Under this formulation ~~, for a completely dry particle~~ $k'_{2f} = 0$ when a particle is completely dry ($[\mathrm{H_2O_{(l)}}] = 0$). ~~In this case, k'_{2f} and therefore $\gamma_{\mathrm{N_2O_5}}$ would also equal 0~~This gives $\gamma_{\mathrm{N_2O_5}} = 0$, and so no $\mathrm{N_2O_5}$ uptake will occur on dry particles.

1.1 Study aims

The Role Of Nightime chemistry in controlling the Oxidising Capacity Of the atmosphere (RONOCO) project was established as a national collaboration of six British universities aiming to better understand nighttime $\mathrm{NO_3}$ radical chemistry, compare its oxidation capacity with that of the daytime OH radical and investigate the impacts of $\mathrm{NO_3}$ chemistry on a regional and global scale. The project consisted of several flight campaigns, carried out over the period of July 2010–January 2011. The July 2010 flights are used for this study, as these had the most complete set of measurements required for analysis of the importance of $\mathrm{N_2O_5}$ heterogeneous chemistry. RONOCO flights were undertaken using the modified Natural Environment Research Council/UK Meteorological Office's BAe 146-301 Facility for Airborne Atmospheric Measurements (FAAM) (Fehsenfeld et al., 2006), which operated out of East-Midlands Airport (52°49′52″ N, 01°19′41″ W), with most flights covering the eastern and southern regions of the UK (see Morgan et al., 2014, for more details). Measurements from these flights have been compared against predictions using the regional Weather Research and Forecasting model with Chemistry (WRF-Chem) model (Grell et al., 2005). This has been modified to include a more detailed treatment of atmospheric oxidative chemistry, including nighttime $\mathrm{NO_3}$ chemistry, its reactions with VOCs, and interactions with aerosol particles via $\mathrm{N_2O_5}$ heterogeneous chemistry (Archer-Nicholls et al., 2014). By comparing the performance of this new version of WRF-Chem with measurement data from the RONOCO flights, this study aims to evalu-

ate current understanding of processes affecting NO_3, and its impact on night-time chemistry throughout north-western Europe.

2 Method

2.1 Instrumentation

The instruments used for this study are summarised in Table 1.

The BBCEAS measures NO_3, N_2O_5, H_2O and NO_2 concentrations to a high level of accuracy (with a detection limit of 1.1 pptv for NO_3), making this campaign the first time simultaneous airborne measurements of NO_3, N_2O_5 and NO_2 have been taken outside of the USA (Kennedy et al., 2011).

Aerosol chemical composition was measured by an Aerodyne compact-Time-of-Flight Aerosol Mass Spectrometer (AMS) (Drewnick et al., 2005; Canagaratna et al., 2007). Specific details relating to the measurements specific to RONOCO can be found in Morgan et al. (2014). The AMS measures non-refractory aerosol species, including organic matter, sulphate, ammonium, nitrate and non-seasalt chloride. Aerosol particles measured by the AMS are assumed to be dry as a result of ram heating of the sampled air flow into the aircraft and the increase in temperature as the sample passes from the cooler ambient environment into the warmer aircraft cabin.

The Thermal Dissociation Laser Induced Fluorescence (TD-LIF) instrument was installed on the FAAM BAe-146 research aircraft to measure NO_2 directly, exciting these molecules with a laser at 532 nm and detecting their fluorescence photons. The TD-LIF measures also total peroxy nitrates ($\sum$PNs, $\sum RONO_2$), total alkyl nitrates ($\sum$ANs, $\sum RO_2NO_2$), and NO_y after thermal dissociation of these species at different temperature (200 °C, 400 °C and 550 °C, respectively) into NO_2 (Di Carlo et al., 2013). To detect simultaneously NO_2, $\sum$PNs, $\sum$ANs, and NO_y the TD-LIF includes four distinct cells one for each of them. The time resolution of the measurements is 10 Hz. The system is equipped with a calibration system to perform in-

flight calibration by injecting a known amount of NO_2 to all cells. More details on the TD-LIF can be found in Di Carlo et al. (2013).

The CIMS instrument has previously been described by Nowak et al (2007) and Le Breton et al. (2012). Its implementation specifically for HNO_3 measurements on board the FAAM BAe-146 research aircraft has previously been described by Le Breton et al. (2013). The air sample is drawn into a $3/8$ OD$''$ diameter PFA inlet heated to $40\,^{\circ}C$ with at a flow of 5.8 SLM. The species of interest are then ionised in the ion molecule region, which is maintained at 19 Torr by a dry scroll pump (UL-DISL 100, ULVAC Industrial). The methyl iodide ionisation scheme is employed here forming an acid-iodine adduct with HNO_3 allowing detection at 190 a.m.u. (Slusher et al., 2004). The resulting ions then pass through a pinhole to an initial octopole, acting as a collisional dissociation chamber. A second octopole collimates the ions which are then mass selected by a quadrupole with pre and post filters. A continuous dynode electron multiplier is utilised for detection. In flight calibrations are performed regularly using a HNO_3 Kin-Tek permeation tube to account for variability in the instrument sensitivity.

2.2 WRF-chem model

WRF-Chem is a fully coupled, "online" regional model with integrated meteorological, gas-phase chemistry and aerosol components (Grell et al., 2005). It is built on the Advanced Research WRF (ARW) core, which handles the meteorology, physics and transport processes. Gas-phase chemistry and aerosol schemes are integrated over the same timestep as the transport processes, allowing for full coupling between the schemes and making studies investigating feedbacks between the chemistry and meteorology possible. The short chemistry timestep also makes the model ideal for studying short-lived species with high levels of spatial heterogeneity.

A number of modifications have been made to WRF-Chem to make it suitable for the RONOCO studies. These include the addition of a reduced version of the Common Representative Intermediates Mechanism (CRIv2-R5) (Jenkin et al., 2008; Watson et al., 2008; Utembe et al., 2009) for gaseous oxidation of VOCs, and the inclusion of the inorganic N_2O_5 heterogeneous chemistry scheme proposed by Bertram and Thornton (2009). These developments are covered in more detail in Archer-Nicholls et al. (2014).

Additional modification of the N_2O_5 heterogeneous scheme has been made to account for the suppression of the uptake of N_2O_5 by an unreactive organic shell around a reactive inorganic core, following the formulation of Riemer et al. (2009). They use a resistor scheme to calculate the reaction probability for the particle:

$$\frac{1}{\gamma_i} = \frac{1}{\gamma_{\text{i,core}}} + \frac{1}{\gamma_{\text{i,coat}}} \tag{6}$$

where $\gamma_{\text{i,core}}$ is the reaction probability of the inorganic core (calculated using Eq. 4), and $\gamma_{\text{i,coat}}$ is the pseudo-reaction probability of the organic shell, calculated following the formulation of Anttila et al. (2006):

$$\gamma_{\text{i,coat}} = \frac{4RTH_{\text{org}}D_{\text{org}}R_{\text{c,i}}}{c_{N_2O_5}l_iR_{\text{p,i}}} \tag{7}$$

where R is the universal gas constant, T is temperature, H_{org} is the Henry's Law constant for N_2O_5 in the organic coating, D_{org} is the diffusion coefficient for N_2O_5 in the organic coating, and $c_{N_2O_5}$ is the average velocity of N_2O_5(g) in the gas-phase. Following Anttila et al. (2006) $R_{\text{p,i}}$, $R_{\text{c,i}}$, and l_i are the radius of the particle, radius of the core, and thickness of the coating, respectively.

H_{org} and D_{org} depend on the physicochemical properties of the compounds comprising the organic coating. Riemer et al. (2009) used values consistent with the analysis presented by Anttila et al. (2006) for these parameters for their modelling work, and their example will be followed below. The product $H_{\text{org}}D_{\text{org}}$ is set to $0.03H_{\text{aq}}D_{\text{aq}}$, where H_{aq} is the Henry's law constant of N_2O_5 for the aqueous phase ($H_{\text{aq}} = 5000\,\text{M}\,\text{atm}^{-1}$) and D_{aq} is the diffusion coefficient of N_2O_5 in the aqueous phase ($D_{\text{aq}} = 1 \times 10^{-9}\,\text{m}^2\,\text{s}^{-1}$).

The composition dependence of $\gamma_{N_2O_5}$ using this combined formulation is illustrated, for a 1 μm diameter particle, in Figure 1. The wholly inorganic, 10% (by molar content) chloride ion scenario (solid red line) gives a rough indication of the upper uptake limit, while the 30% (by mass) organic matter (OM) particle composition scenarios (all dotted lines) give a rough indication of the lower uptake limit.

2.3 Model configuration

This study uses a single domain, with 15 km horizontal grid spacing and a size of 134 (E–W) by 146 (N–S) grid points, by 41 vertical model levels, covering the UK and much of N–W Europe (cf. Fig. 3a). Meteorological boundary conditions were taken from ECMWF ERA-Interim reanalysis data (Dee et al., 2011). Gas-phase chemical boundary conditions were taken from the global Model for Ozone and Related Chemical Tracers (MOZART-4) (Emmons et al., 2010), while the global Monitoring Atmospheric Composition and Climate (MACC) model (Stein et al., 2012; Inness et al., 2013) was used for aerosol boundary conditions. Anthropogenic emissions are taken from the UK National Atmospheric Emissions Inventory (NAEI) (http://naei.defra.gov.uk) and the TNO emissions inventories Denier van der Gon et al. (2010). Biogenic emissions were calculated "on-line" using the Model of Emissions of Gases and Aerosols from Nature (MEGAN) V2.04 (Guenther et al., 2006; Sakulyanontvittaya et al., 2008). DMS emissions from the sea-surface are calculated assuming a constant oceanic DMS concentration of $2\,\mathrm{nM\,L^{-1}}$ (representing low-level background activity, as estimated from the database of Kettle et al., 1999). Domain configuration and inputs are described in more detail in Archer-Nicholls et al. (2014). The configuration of WRF physical parameterisations used for this study is given in Table 2. The gas-phase chemistry scheme used is CRIv2-R5 (as described above); we use the MOSAIC module to represent aerosol chemistry (Zaveri et al., 2008), configured with 8 size-bins and coupled to the aqueous-phase chemistry. Sea-spray emissions are treated using the modified scheme described in Archer-Nicholls et al. (2014), based on Gong et al. (1997) and Fuentes et al. (2011), using the default low-biogenic activity scenario.

Four scenarios have been run to investigate the importance of N_2O_5 heterogeneous chemistry, the details of which are given in Table 3. Each scenario was run from 00:00 UTC on the 10 July 2010 to 12:00 UTC on the 30 July 2010. This covers the RONOCO summer flight campaign, with five days of spin up for the chemistry. The size of the model domain was such that the boundary conditions provided sufficient guidance (without explicit nudging within the domain) for divergence from the ECMWF reanalysis data to not be significant. The only restart

of the meteorological fields, implemented because of divergence from the ECMWF reanalysis data at this date, was at 00:00 UTC on the 21 July 2010 (chemical and aerosol tracers were carried through continuously).

3 Results and discussion

There were 8 flights during the RONOCO summer campaign (numbered B534–B542; without B540, which was aborted early). For three of these flights (B534, B536 and B537) the modelled specific (and relative) humidities along the flight path diverge too much from the measurements for the data to be useful in studying the importance of heterogeneous chemical processes (these discrepancies persisted even when the meteorological variables were reinitialised within 48–24 h of the start of the flight). The meteorological match between the model and measurements along the aircraft flightpath are reasonable for the remaining flights, although it should be noted that previous studies of WRF simulations in the region of N–W Europe have identified systematic biases in the model meteorological fields (García-Díez et al., 2013; Krogæter and Reuder, 2014). These biases will be discussed in Sect. 3.1, and their potential impacts on the chemistry simulations will be discussed in the relevant sections below.

The analysis in this paper will concentrate on two flights: B535 (on the 17 and 18 July), which flew over the North Sea (off the east coast of England) (Fig. 2a); and B541 (on the 29 July), which predominately flew over the English Channel (off the south-east coast of England) (Fig. 2c). These are the flights with the most complete datasets (CIMS HNO_3 data are not available for B539, while BBCEAS N_2O_5 data are not useable in the latter half of B542) and for which WRF-Chem best captures the core atmospheric chemical properties (modelled NO_2 mixing ratios during the first half of flight B538 are significantly lower than the measured NO_2 mixing ratios, a discrepancy which exists in all model scenarios and would complicate the analysis of the impacts of N_2O_5 heterogeneous chemistry). Flight B535 was designed to measure the pollution plumes from cities on the east coast of northern England, advected across the North Sea by a westerly zonal flow. Flight B541 was designed to measure the overall pollution from emissions across the whole of the UK which accumulated in the air masses advected

across the English Channel in a northerly mean flow. Both flights principally consisted of level flights at around 500 m altitude (960 hPa pressure level) over open water (due to night-time air traffic restrictions), with occasional climbs to investigate elevated pollution layers (see Morgan et al., 2014, for more details on experimental procedures).

In the first section the meteorological conditions during the periods of the two test flights is examined (a more general overview of the meteorological conditions during the campaign is presented in Morgan et al., 2014); while the second section gives an overview of the chemistry over the UK region during the two flights. These are followed by a statistical comparison of the measured and modelled chemical species along the flight-paths. The section on the impacts of N_2O_5 heterogeneous chemistry starts with an examination of the implications for NO_3 and N_2O_5 mixing ratios, and the dependence of this process on local meteorological conditions, followed by an examination of the influence on particulate nitrate mass loadings and gas-phase HNO_3 mixing ratios. The final section investigates the regional impacts of these processes – looking at the mass loadings of aerosol nitrate, and impacts on gas-phase oxidative capacity of the atmosphere.

1 min averaged measurement data is used for the following analysis. Throughout all model runs, WRF-Chem data is output hourly (on the hour) for the whole domain. The aircraft GPS latitude and longitude at the mid-point of each 1 min measurement period was used to find the model grid column in which it is located, and the model data were interpolated to the aircraft pressure level within that column. From each of the hourly model outputs data were extracted along the flight path for 45 min before and after the model output time, providing up to 90 data points per output file, with a 30 min overlap in model data in-between each hour (offering some indication of the temporal variation within the model). In the flight-path analysis plots the model data for each hour is plotted as a separate coloured line (the model time indicated in the legend text).

3.1 Meteorology

On the 17 July the presence of low pressure systems in the Bay of Biscay and to the north of Scotland led to strong, near zonal, air flow over the UK. Bands of frontal rain passed over

the UK on the 17th and 18th – flight B535 was conducted during a dry period between these events. Figure 3a shows the modelled radar-derived rain rate, and wind vectors interpolated to the 960 hPa pressure level, at 00:00 UTC on the 18 July. The B535 flight region is dry, matching NIMROD radar-derived rainfall rates (see Supplement). The match between the model and measurements is not perfect: the frontal system which lies over Ireland and western Scotland in the model is shown to actually lie further south (lying over Wales) in the measurements. Along the flightpath, however, the modelled meteorological variables show quite similar behaviour to the measured meteorology. The modelled temperature fields follow the measured values, although they are generally 1–2 K lower (Fig. 3c). Specific humidity values are very similar between model and measurements, though the model shows larger variety along the flat and level sections of the flight (see Supplement). The low temperature impacts on the relative humidity, this is a little higher (by 5–10 %) than the measurements, however they both lie between 50–70 % in the first section of the flight, and 60–80 % in the second section of the flight (Fig. 3e). Wind speed and direction are very similar, around 5–10 $\mathrm{m\,s^{-1}}$ and mainly westerlies (see Supplement). The greatest discrepancy between model and measurements occurs during the mid-flight climb (shortly after 23:00 UTC, Fig. 2b): the potential temperature increases, and specific humidity decreases, much further at 850 hPa in the model than in the measurements, and shows more similarity to the values at 800–750 hPa than at 960 hPa indicating that the modelled boundary layer is too shallow.

During the period leading up to flight B541 there was less rainfall over the UK than before flight B535. A low pressure system over Scandinavia, combined with high pressure over the Bay of Biscay, led to a north-westerly air flow along the length of the UK on the 28 July (Fig. 3b). During the period of flight B541 most of the UK was dry – only a few scattered showers exist over the English Channel (see Supplement and Fig. 3b). During the flight agreement between the modelled and measured meteorological variables is lower than during flight B535. Modelled temperature is, again, 1–2 K lower than the measurements (Fig. 3d). During this flight, at low altitudes, the modelled specific humidity is slightly higher than measured (see Supplement), and the combination of this bias with the low bias in air temperature, leads to consistently higher modelled relative humidities (80–100 %) compared with the measurements (70–90 %) (Fig. 3f)

during much of the flight. Model and measurement wind directions are very similar, both north-westerlies along the majority of the flat and level flight sections. Modelled wind speeds are consistently lower in these sections, around 6–8 $\mathrm{m\,s^{-1}}$, compared with measured wind speeds of around 10 $\mathrm{m\,s^{-1}}$, although the modelled wind speeds at higher altitudes (above 750 hPa) are significantly higher than the measurements (see Supplement).

The differences between modelled and measured meteorological variables along the aircraft flightpath in this study are typical of those observed in previous WRF studies over N–W Europe. García-Díez et al. (2013) ran meteorological simulations across the whole of Europe using WRF 3.1.1, with similar physical parameterisations to the setup used in this paper (specifically using the NOAH land-surface model, and MJY planetary boundary layer (PBL) scheme). They found systematic cold biases (with a mean of $-0.8\,\mathrm{K}$ at 925 hPa) and higher specific humidities (with a mean of $+0.0005\,\mathrm{kg\,kg^{-1}}$ at 925 hPa) across Europe in the model, during the summer months, compared to atmospheric soundings. They concluded that PBL schemes within WRF generally underestimate entrainment between the PBL and free troposphere (FT). This finding is re-enforced by the study of Krogæter and Reuder (2014), who investigated the performance of PBL schemes in WRF 3.2.1 over the North Sea by comparing model results with measurements taken from the FINO1 platform during 2006 (located at 54.01° N, 6.59° E, about 45 km north of the German coast). They found that all PBL schemes over-predicted the frequency of stable and neutral conditions during the summer months, while under-predicting the frequency of unstable conditions. The MJY scheme was one of the better performing PBL schemes, however it still generally predicted lower PBL heights than those determined from the measurements, and forecast frequencies of unstable or very unstable conditions of only 0.25 during July (compared with measured frequencies of 0.45). The implications of these meteorological biases in the model on the chemistry fields will be discussed below.

3.2 Regional chemistry over the UK

An aim of the RONOCO campaign was to sample the chemical space of N–W Europe as representatively as possible. To illustrate the model chemical space, two-dimensional histograms of NMVOC:$\mathrm{NO_x}$ space during the periods of flights B535 and B541 are shown in Fig. 4. Data is

taken from the whole domain (less 10 grid cells around the edge of the domain), interpolated to 960 hPa pressure level. The density maps for both flight periods are, roughly, bi-modal (more so for the B541 period, but this holds true for the B535 period too): a mode below 100 pptv of NO_x represents clean conditions, principally observed in the north-western part of the domain (over the Atlantic Ocean); a second mode, which peaks around 1000 ppt of NO_x, but extends up to 10 000 ppt of NO_x, represents the regional pollution haze which lies over the majority of continental N–W Europe (and extends over the North Sea and UK). Model data along the paths of both flights (between 950–970 hPa) are represented by black stars. Both flights are focussed on the polluted regions of the domain (as per the aims of campaign), with NO_x mixing ratios generally between 1000–10 000 pptv, although during B535 there is more heterogeneity, as the aircraft sampled cleaner air over the North Sea.

The differences between the flights are observable in the spatial distribution, and temporal evolution, of NO_2, NO_3 and N_2O_5, shown in Figs. 5 and 6 for flights B535 and B541, respectively. The left-most six panels in each show the horizontal distribution (from the "het on" model scenario) for these species at the times of 23:00 and 00:00 UTC through the night of the 17–18 July (interpolated to the 970 hPa pressure level) for flight B535, and at the times of 00:00 and 01:00 UTC through the night of the 28–29 July (interpolated to the 960 hPa pressure level) for flight B541. The flight track is shown as a thick black line, superimposed with measurement data for $\pm$30 min around the model output time, and for $\pm$10 hPa around the plotted pressure level. The right-most three panels show the vertical distributions of these species along the flight path, composed of data from each of the hourly output files (extracted along the flight path $\pm$30 min either side of the hour), giving an indication of both the vertical spatial and temporal variations in the model fields. Again the flight path is plotted as a thick black line, with the measurement data (where available) superimposed on this line. Similar plots for the "no Cl pathway", "organic suppression", and "het off" scenarios are included in the Supplement.

Flight B535 sampled plumes of pollution carried out over the North Sea, from UK sources, by the prevailing westerlies. The largest plumes of NO_2 predicted by the model are at 51.5 and 54° N, reaching peaks mixing ratios of 3–4 ppbv and 5–6 ppbv respectively (cf. Fig. 5a and b). These peak mixing ratios are lower than the maximum measured NO_2 mixing ratios (which

reach 8–9 ppbv), however the model is managing to get the location of the plumes reasonably correct. The vertical distributions NO_2 along the flight path (Fig. 5c) show quite a strong vertical gradient within these plumes. For the first, southerly, plume (which the aircraft flew through around 22:30 UTC, performing a deep vertical profile over London-Southend airport), the modelled mixing ratios are significantly higher than the measured values. For the second, northerly, plume (which the aircraft flies through three times: around 23:40, 23:50, and 00:25 UTC) the model shows a strong vertical gradient in NO_2 close to the coast (reaching over 10 ppbv below 980 hPa around 00:30 UTC); further from the coast, however, (around 23:40 UTC) the model mixing ratios are much lower, even at ground level (only reaching 6–7 ppbv). It is probably that the 15 km resolution grid used for this study is too coarse to properly represent this narrow plume.

Through the night the NO_3 mixing ratios steadily increase, from peaks of 20–30 pptv at 22:00 UTC (Fig. 5f) up to peaks of 70–100 pptv at 01:00 UTC (see Supplement). NO_3 concentrations over 10 pptv extend, in places, above 850 hPa (principally in the early part of the flight, below 52° N); later in the flight, in the more northerly sections, the vertical extent of NO_3 is lower. NO_3 mixing ratios are greatest between 990–970 hPa, at 00:00 UTC the model predicts peak NO_3 mixing ratios of 50–70 pptv at these altitudes (Fig. 5e). The measured NO_3 mixing ratios are of a similar magnitude to the model predictions, but reach lower peak values of only 30–50 pptv (cf. Fig. 5d–f). This is to be expected, since the aircraft is flying slightly above the pressure levels at which predicted peak NO_3 mixing ratios occur, as well as earlier than the period of highest NO_3 mixing ratios (which occur after 01:00 UTC).

N_2O_5 mixing ratios increase through the night in a similar manner to the NO_3 mixing ratios (cf. Fig. 5g and h), reaching peak values of 500–700 pptv. The distribution of N_2O_5 strongly follows the distribution of NO_2 (more so than NO_3) because the formation of N_2O_5 is second order dependent on $[NO_2]$~~)~~. In the northern plume, N_2O_5 mixing ratios are greatest further from the coast (around 23:40 and 23:50 UTC, compared with 00:25 UTC; Fig. 5i), this is because the NO_3 mixing ratios close to the coast are low (cf. Fig. 5f) so N_2O_5 also cannot form.

During the period of flight B541 NO_2 is, in the model, principally concentrated over the English Channel and northern France, reaching peaks of 8–9 ppbv in plumes rising over north-

ern France, and is generally around 1–3 ppbv in the region of the flight (Fig. 6a and b). NO_2 mixing ratios are generally higher at ground level, below the aircraft, during this flight than during B535 (Fig. 6c); principally this is due to the English Channel having more concentrated shipping lanes than the North Sea. The vertical distribution of the plumes of NO_2 is shallower than during B535, generally not extending much higher than 900 hPa. NO_3 distributions exhibit a non-linear relationship with NO_2: the highest mixing ratios (up to 20–50 pptv) occur where NO_2 mixing ratios are around 1–2 ppbv, but drop off rapidly to 3–5 pptv where NO_2 (roughly) drops below 0.5 ppbv or increases above 7 ppbv (Fig. 6d and e). This relationship is driven by the necessity of having NO_2 to produce NO_3, but then at too high concentrations the reaction of NO_2 with NO_3 titrates it away to form N_2O_5 (the distribution of which follows that of NO_2; Fig. 6g and h). NO_3 is also predominately concentrated below 900 hPa, but in places there are plumes around 820–850 hPa (Fig. 6f). N_2O_5 plumes are principally constrained below 900 hPa, with mixing ratios peak at only 300–500 pptv during this flight (Fig. 6i).

3.3 Statistical measurement–model comparison

Model data has been extracted along the flight path in the manner described at the start of Sect. 3. For statistical analysis of the results, the same model data extraction technique has been used (but only for $\pm$30 min each side of the hour, to avoid duplications in the model-measurement comparison), selecting only the data above the 980 hPa pressure level (giving 241 and 265 potential data points for flights B535 and B541, respectively), using data points where measurement data exists, and is above the quoted instrument detection limits. While doing this could lead to a bias in the statistical analysis, it is a necessary step in processing the data, and for most species less than 10–20 data points have been discarded due to this cut-off. The fewest data points used for the analysis below are 154 and 153, for NO_3 and N_2O_5 respectively, during flight B535, due to gaps in the measurement dataset rather than from eliminating data below the instrument detection limits.

The mean values and standard deviations for the measurement and model data are calculated, along with the correlation coefficient (CORR) and root-mean-square (RMS) difference between the measurements and each model scenario. The mean values are plotted in side-panels to the

left of the time-series plots of the measurement, and "het on" model scenario, data. The rest of the statistical diagnostics are plotted using Taylor diagrams (Taylor, 2001) in the right-hand side panels. Measurement data is shown by a red circle; the "het on", "no Cl pathway", and "het off", model scenarios are represented by a black circle, cross, and diamond, respectively. The radial distance between each symbol and the origin is proportional to the standard deviation (sd) of that dataset, while the azimuthal positions give the correlation with the measurements. The dashed green lines measure distance from the measurement data point, which is proportional to the RMS difference.

Comparisons of NO_3, N_2O_5, NO_2, and O_3 mixing ratios between measurements and the "het on" scenario are shown in the main panels of Fig. 7, for flight B535, and Fig. 8, for flight B541. During both flights the model matches the mean NO_2 and O_3 mixing ratios well, as well as capturing the strong vertical gradient in O_3 mixing ratios (giving correlations of 0.8–0.9 with the measurements). As noted above however, these stats are calculated just using data from above 980 hPa. During the deep vertical profile around 22:30 UTC, modelled O_3 mixing ratios drop below 10 ppbv, and at the start and end of the flight they are almost zero. During the deep vertical profile the 1 min averaged O_3 measurements drop no lower than 25 ppbv, and at ground level they are no lower than 20 ppbv. We treat all NO_x emissions as NO in our model setup, at night-time the rapid reaction of NO and O_3 would lead to the over-destruction that we observe in the model. However it should be noted that the modelled mixing ratios of NO_2 are also very high close to the ground (22 ppbv during the deep vertical profile at 22:30 UTC during Flight B535, compared with 1 min averaged measurements of 10 ppbv), while we are not able to replicate the magnitude of NO_2 plumes at altitude (cf. the plume around 23:40 UTC, with measurements of 10 ppbv NO_2, and modelled values of less than 5 ppbv). This suggests that the low entrainment between PBL and FT in WRF noted in Sect. 3.1 may be too strongly limiting the vertical mixing of pollutants within (and out of) the PBL during the night. Such unrealistic build up of high concentrations of pollutants in the nighttime marine PBL (off the north-eastern coast of the USA) within WRF-Chem has been previously identified, and attributed to the PBL scheme being too stable, by McKeen et al. (2007). The spikes in NO_2 mixing ratios due to the pollution plumes during flight B535 (Fig. 5a–c) are roughly co-incident with troughs in

the O_3 mixing ratios (Fig. 7c and d). However, because the plumes in the model are displaced compared to the measurements, as noted in the previous section, correlation between the model and measurements is poor (0.3–0.4). During flight B541, which sampled a widespread, well mixed, layer of pollution, correlation between the model and measurements is a lot higher (0.7), although the model shows greater variability, due to a few NO_2 plumes pushing up through the flight altitude from the planetary boundary layer (cf. Fig. 6c).

During flight B535 the mean measured NO_3 and N_2O_5 mixing ratios were 23 and 150 pptv respectively (dashed blue lines in Fig. 7a and b). As described above, NO_3 measurements show low variability, the sd is only 7 pptv; however N_2O_5 variability is higher, with a sd of 160 pptv. During flight B541 the NO_3 and N_2O_5 mixing ratios were generally lower, with means of 11 and 86 pptv respectively, with low variability too (Fig. 8a and b). The modelled mean values for NO_3 and N_2O_5, during flight B535, for all model scenarios are close to, though slightly higher than, the measurements; however correlation between the model and measurements are low, around 0.3–0.4 for NO_3 and 0.1–0.2 for N_2O_5 due to the spatial heterogeneity of the pollution plumes.

During flight B541 there is high correlation between model and measurements for N_2O_5 (0.8) (Fig. 8b), as it's mixing ratio is principally altitude-dependent during this flight, and so is captured well by the model. Correlation between model and measurements for NO_3 is poor (0.2–0.4) (Fig. 8a), however the periods during which correlation is poor generally correspond to large changes in altitude (cf. the periods immediately after 23:00 and 03:00 UTC) which can cause baseline drifts in the NO_3 measurements. N_2O_5 measurements are generally less affected by this drift due to: (i) the (generally) larger mixing ratios; and (ii) the N_2O_5 cavity was thermally maintained at a fixed temperature and so has been found to resist temperature drift (due to rapid change in temperature of the incoming sample gas) better. There are large differences in mean values and standard deviation for NO_3 and N_2O_5 predictions by the different model scenarios during this flight. The causes of these will be discussed in the next section.

Comparisons of AMS measurements of inorganic aerosol species are compared with "PM_1" aerosol data from the model (the sum of the smallest 4 size bins in the model, plus 0.678 of the 5th size bin), as well as CIMS measurements of HNO_3 with modelled HNO_3 mixing

ratios, for B535 and B541 are presented in Fig. 9). For both flights, AMS measurements of aerosol sulphate and ammonium suggest the existence of widespread homogeneous aerosol fields, around the 950–960 hPa pressure level, with mean mass loadings of 1.3 and 1.2, and 0.5 and 0.9 $\mu g\,kg_{air}^{-1}$, respectively (Fig. 9e–h). Throughout the campaign the model underpredicts the PM_1 sulphate mass loadings (with means of 0.5–0.7 $\mu g\,kg_{air}^{-1}$), and shows no correlation with the measurements. It is unclear what is the cause of the under-prediction of sulphate – perhaps the general underestimation of entrainment between the PBL and FT in WRF noted in Sect. 3.1 prevents sufficient transport of aerosol out of the PBL, or given the homogeneous nature of the measurements it is possible that we are missing broad background aerosol fields from our boundary conditions – further investigation is needed into this.

The low model prediction of sulphate aerosol also lead to low ammonium aerosol mass loadings (means of 0.2–0.4 $\mu g\,kg_{air}^{-1}$). During B535 PM_1 ammonium is more closely associated with PM_1 nitrate aerosol (cf. Fig. 9c and g). During flight B541 this is also true, but PM_1 ammonium mass loadings are also limited by the availability of gas-phase ammonia. The total system mass loading of potential ammonium (gas-phase NH_3 plus PM_{10} ammonium) along the flight track in all model scenarios is lower than the AMS measurements of PM_1 ammonium (not shown). The ~~low sulphate content~~ lower sulphate to ammonium ratio of the PM_1 aerosol in the model ~~also leads to a~~ leads to the model chemistry being less ammonia-limited than in reality. This allows for a higher PM_1 chloride content ~~than have been~~ in the model than was measured (model means of 0.1–0.4, compared with measurement means of 0.04–0.06 $\mu g\,kg_{air}^{-1}$, see Supplement). Generally this is in the form of sodium chloride, but for particles below a diameter of around 0.3 µm (MOSAIC size bins 1–3) there is significant ammonium chloride as well, created by the co-condensation of hydrochloric acid with ammonia.

During flight B535 modelled PM_1 nitrate mass loadings, and gas-phase HNO_3 mixing ratios, are much higher than the measurements. Measured means are 0.17 $\mu g\,kg_{air}^{-1}$ and 130 pptv, compared with modelled means of 0.4–0.7 $\mu g\,kg_{air}^{-1}$ and 240–300 pptv, respectively (Fig. 9c and a). The consistency of this discrepancy across all the model scenarios indicates that it is caused by daytime nitrate production over the UK; the simulations show the formation of plumes of HNO_3 over northern England during the afternoon, which are then advected across to the flight region

(see Supplement). It is likely that the meteorological conditions in reality were different enough to the model that either these plumes did not form, or they were transported to a different part of the domain, and so were not sampled by the aircraft.

PM_1 nitrate and HNO_3 measurements are higher during B541 (means of 1.7 $\mu g\,kg_{air}^{-1}$ and 270 pptv, respectively). PM_1 nitrate shows a lot of variability (sd of 1.3 $\mu g\,kg_{air}^{-1}$; Fig. 9d), consistent with pollution plumes; however HNO_3 has much lower variability than would be expected through the flight (sd of 50 pptv; Fig. 9b), the causes of which are not clear. PM_1 nitrate model predictions are much lower than the AMS measurements, with strong dependencies on the chemical scenario, as discussed below. HNO_3 model predictions are of a similar magnitude to the measurements, but exhibit the same strong variability as modelled and measured PM_1 nitrate.

3.4 Impact of N_2O_5 heterogeneous chemistry

In this section the impacts of N_2O_5 heterogeneous chemistry on NO_3, N_2O_5, HNO_3 and particulate nitrate are investigated by comparing the results from the different model scenarios. ~~It was found that the magnitude of the suppression of by an organic shell was such that the~~ The results from the "organic suppression" scenario were ~~very similar~~ similar to those from the "het ~~off" scenario(Morgan et al., 2014, also found that the organic shell parameterisation suppressed $\gamma_{N_2O_5}$ too~~ on" scenario, though the "het on" scenario results are generally a better fit to the measurements (see discussion below). The organic mass fractions of the aerosol in the model are significantly lower than those measured by the AMS instrument, resulting in far lower suppression of the N_2O_5 uptake coefficient than that calculated from the measured aerosol compositions (Morgan et al., 2014) . Because of this discrepancy the results of the "organic suppression" scenario have been included in the Supplement, but are not discussed below.

3.4.1 Impacts on NO_3 and N_2O_5

During flight B535 all model scenarios predict similar NO_3 and N_2O_5 mixing ratios to the measurements. The "het on" and "no Cl pathway" scenarios are closest, at 25–26 pptv for NO_3

and 200 pptv for N_2O_5. "het off" scenario mean values are higher, at 30 pptv for NO_3 and 250 pptv for N_2O_5. Sd values for NO_3 are high in all scenarios, around 10–12 pptv (the "no Cl pathway" scenario is lowest), indicating that there is greater spatial heterogeneity of NO_3 in the model than in the measurements. Sd values for N_2O_5 in the "het on" and "no Cl pathway" scenarios are close to 150 pptv, but, again, higher in the "het off" scenario, at around 190 pptv. These differences between the "het off" and other scenarios show that N_2O_5 heterogeneous chemistry is suppressing the build up of N_2O_5 in the plumes (but these are always too diffuse in the model, leading to higher background mixing ratios of N_2O_5 around the plumes). N_2O_5 heterogeneous chemistry is also suppressing the regional build up of NO_3. However, because relative humidity is low during this flight, the suppressive effect of N_2O_5 heterogeneous chemistry is not particularly strong. During flight B541 model predictions of NO_3 and N_2O_5 for the "het on" and "no Cl pathway" scenarios are very similar to the measurements, with mean values of 9.5–10 and 69–72 pptv, and sd values around 5 and 60 pptv, respectively. However, predictions of NO_3 and N_2O_5 are much higher in the "het off" scenario, with mean mixing ratios of 27 and 233 pptv, and sd values of 17 and 200 pptv, respectively. Without the suppressive effect of N_2O_5 heterogeneous chemistry the NO_3 and N_2O_5 mixing ratios also increase through the night, in a similar manner to their behaviour during flight B535 (see Supplement).

For both testcases described above the inclusion N_2O_5 heterogeneous chemistry improves the model prediction of NO_3 and N_2O_5 mixing ratios (although there is little to distinguish between the "het on" and "no Cl pathway" scenarios). The clearest dependence for the effectiveness of N_2O_5 heterogeneous chemistry is on the atmospheric relative humidity. For the majority of flight B535 this is around 60–70 % (Fig. 3e), and while N_2O_5 heterogeneous chemistry does limit NO_3 and N_2O_5 mixing ratios, it does not have a very strong influence (Fig. 7a and b). In contrast, during B541 relative humidity levels are around 80–90 % (Fig. 3f), and N_2O_5 heterogeneous chemistry has a far stronger effect on NO_3 and N_2O_5 mixing ratios (Fig. 8a and b). The high aerosol nitrate mass loadings in the model (compared to measurements) during B535 will contribute to the suppression of $\gamma_{N_2O_5}$. However the nitrate mass loadings are similar to those observed during B541, when there is little suppression of $\gamma_{N_2O_5}$, and so it is evident that relative

humidity (and so aerosol water content) is still the most important factor for determining $\gamma_{N_2O_5}$ in these cases.

Many previous studies into N_2O_5 heterogeneous chemistry have observed low $\gamma_{N_2O_5}$ values, with no dependence on RH. The studies have, however, mostly been at lower RH values with high organic particulate mass fractions, e.g.: Zaveri et al. (2010a), who concluded that $\gamma_{N_2O_5}$ was likely to be negligibly small (< 0.001) within power plant plumes with organic aerosol mass fractions around 60–80 %, at an RH of 60–70 %; and Brown et al. (2009), who reported $\gamma_{N_2O_5}$ values below 0.01, with no RH dependence, for organic aerosol mass fractions of 50–70 % and principally in the RH range of 35–75 %; similarly, Zaveri et al. (2010b) concluded that $\gamma_{N_2O_5}$ was likely on the order of 0.001 for the organic-rich aerosol in the Houston urban/industrial plume. Brown et al. (2006) also report low $\gamma_{N_2O_5}$ values (0.001) where the organic aerosol mass fraction was roughly 50 %, and RH was 44–52 %. Higher $\gamma_{N_2O_5}$ values (0.017) are observed where the organic mass fraction is a lot lower (< 30 %), however they do not report any RH values for this period of the flight. The most comparable previous study with this one was carried out by Bertram and Thornton (2009) near Seattle. This study was at an enhanced RH (74 ± 13 %) compared to many of the investigations above, leading to greater hygroscopic growth of the aerosol, and they reported high $\gamma_{N_2O_5}$ values (0.005–0.03) with a strong positive correlation with RH. This is similar to the importance of RH observed in flights B535 and B541.

Because of this relationship, when the meteorological conditions are wrong in the model the influence of heterogeneous processes will be strongly impacted. For example, relative humidity levels are very high in all model runs in the region of flight B534 (flown through the night of the 16–17 July), around 90–100 % RH, compared with in-flight measured RH levels of 60–80 % (Fig. 10c). This difference is driven by the greatly increased specific humidity ratios in model ($0.009\,\mathrm{kg\,kg^{-1}}$, as opposed to measured ratios of $0.007\,\mathrm{kg\,kg^{-1}}$; Fig. 10d). The high RH levels within the model lead to very strong suppression of NO_3 and N_2O_5 mixing ratios in the "het on" and "no Cl pathway" scenarios (Fig. 10a and b). It is the "het off" scenario which best matches the magnitude and variability of the measurements, with respective mean values of 30 and 250 pptv (compared with measured means of 26 and 190 pptv), and sd values of 13 and 179 pptv (compared with measured sd's of 13 and 200 pptv), respectively.

3.4.2 Impacts on particulate nitrate and gas-phase HNO_3

As noted in Sect. 3.3, model predictions of gas-phase HNO_3 and PM_1 nitrate do not match measurements particularly well. During flight B535 model predictions of both are high (due to daytime production) – N_2O_5 heterogeneous chemistry does cause increases in the modelled PM_1 mass loadings, however these are small (Fig. 9c). Likewise there is no systematic response in HNO_3 mixing ratios to N_2O_5 heterogeneous chemistry during this flight (Fig. 9a).

During flight B541 N_2O_5 heterogeneous chemistry is a lot more efficient, as noted above, and so has a stronger influence on model predicted gas-phase HNO_3. This leads to increases from a mean of 50 pptv in the "het off" scenario up to means of 180 and 160 pptv for the "het on" and "no Cl pathway" scenarios, respectively. Although these means are close to that of the HNO_3 measurements, the model variability is much greater than the measured variability, and is instead more consistent with the PM_1 nitrate plumes (Fig. 9b). PM_1 nitrate model predictions are much lower than the AMS measurements in all scenarios. The mean mass loading in the "het off" scenario is 0.8 $\mu g\,kg_{air}^{-1}$, N_2O_5 heterogeneous chemistry increases this, but more so for the "no Cl pathway" scenario (which increases the mean to 1.4 $\mu g\,kg_{air}^{-1}$ and the sd doubles to 0.9 $\mu g\,kg_{air}^{-1}$) than for the "het on" scenario (for which the mean only increases to 0.9 $\mu g\,kg_{air}^{-1}$). This suggests that N_2O_5 heterogeneous chemistry is preferentially occurring on the coarse-mode sea-salt particles in this model scenario (which will be explored below). In all model scenarios, however, the potential PM_{10} nitrate (HNO_3 plus PM_{10} nitrate) is lower than the summed CIMS + AMS potential PM_1 nitrate (not shown). This shows that the shortfall in PM_1 nitrate mass within the model, compared with the measurements, cannot only be due to the differences between the real and modelled aerosol size and composition distributions. A similar shortfall to that observed in the modelled potential ammonium during this flight described in Sect. 3.3.

As an illustration of the regional influence of N_2O_5 heterogeneous chemistry on aerosol nitrate formation, the spatial distributions of PM_1 nitrate in the three model scenarios for Flight B541 are shown in Fig. 11. In all scenarios PM_1 nitrate is highest over the English Channel and across northern France (at the pressure level 960 hPa); along the flight path (principally

over the English Channel) PM_1 nitrate is concentrated below 880 hPa. In the "het on" (Fig. 11a and b) and "het off" (Fig 11e and f) scenarios the maximum PM_1 nitrate mass loadings are generally between 1–2 $\mu g\, kg_{air}^{-1}$ – only over northern France do the PM_1 nitrate mass loadings get over 2 $\mu g\, kg_{air}^{-1}$ (Fig. 11a). PM_1 nitrate mass loadings are generally higher in the "no Cl pathway" scenario (Fig. 11c and d), mass loadings greater than 1 $\mu g\, kg_{air}^{-1}$ are more widespread, in several locations it gets up to 2–3 $\mu g\, kg_{air}^{-1}$. In both the "het on" and "no Cl pathway" scenarios the vertical distribution of PM_1 nitrate is higher than in the "het off" scenario. In the "no Cl pathway" scenario the PM_1 nitrate mass loadings are increased (in comparison with the "het off" scenario) at all model levels, however in the "het on" scenario the PM_1 nitrate mass loadings are lower at low altitudes (in comparison with both the "no Cl pathway" and "het off" scenarios). In none of the scenarios do we have sufficient model PM_1 nitrate (compared with AMS nitrate measurements) within the region of the flight.

Spatial distributions of PM_{10} nitrate are similar to those of PM_1 nitrate (see Fig. 12). Mass loadings are highest in the "no Cl pathway" scenario, with peaks greater than 5 $\mu g\, kg_{air}^{-1}$ over northern France. Mass loadings in the "het on" scenario are now clearly greater than those in the "het off" scenario, both at higher altitudes and close to the ground surface, indicating that N_2O_5 heterogeneous chemistry at low altitudes over the sea is being driven by reactions on large sea-salt particles. In the "no Cl pathway" scenario there is, in places, as much PM_{10} nitrate in the model as in the AMS nitrate mass loading measurements, however the mass loadings in the "het on" scenario are still low (and there is definitely not enough in the "het off" scenario).

Ground-based measurements of size-resolved inorganic aerosol compositions across both Europe and the USA show that condensed-phase sulphate and ammonium are generally concentrated in the accumulation mode, while condensed-phase nitrate is more evenly distributed between the accumulation and coarse modes (Wall et al., 1988; John et al., 1990; Neusüßet al., 2002; Putaud et al., 2004). Close to the coast, where sea-salt particles predominate the aerosol population, most nitrate is in the coarse mode (cf. Wall et al., 1988; Putaud et al., 2004) – further in-land, where other aerosol emission sources dominate, most nitrate is in the accumulation mode, although still a significant fraction remains in the coarse mode (cf. John et al., 1990; Neusüßet al., 2002). In our simulations the fractional content of aerosol nitrate in the

super-micron particles (along the B541 flight path) is between 0.3–0.6 (not shown). While the distribution of nitrate across the aerosol size range is consistent with these previous measurement studies, it should be noted that the under-prediction of sulphate in the model reduces the surface area in the accumulation mode, and the coarse mode contribution at the flight altitudes to aerosol surface area is higher in the model (up to 10 %) compared with the measurements (around 1 %) (see Supplement). These differences in the aerosol distribution could potentially lead to more nitrate condensing onto the coarse mode at these high altitudes in the model than would actually occur in reality.

3.5 Regional influences on nitrate formation and oxidation budgets

In the previous sections the localised impacts of N_2O_5 heterogeneous chemistry have been investigated. The flights sampled air which, the model predicts, was representative of the pollution coming off the UK (Fig. 4). To investigate the regional impacts of N_2O_5 heterogeneous chemistry model predictions from across the whole domain (minus 10 grid cells around the edge of the domain, to avoid boundary effects) are used. This captures both the behaviour of the pollution fields over the UK, mainland Europe, and North Sea, as well as the cleaner air over the Atlantic Ocean and the Bay of Biscay.

The daytime formation of nitrate from the $NO_2 + OH \rightarrow HNO_3$ reaction creates a strong diurnal cycle in the atmospheric nitrate mass loadings. ~~This~~ For this reaction the three-body rate recommended by DeMore et al. (1994) is used, which gives a reaction rate (at a pressure of 1 atmosphere, and a temperature of 285 K) of 1.28×10^{-11} molecules^{-1} cm^3 s^{-1}. This diurnal cycle can be observed in the tendencies of the total (condensed-phase nitrate plus gas-phase HNO_3) nitrate mass loadings in the "het off" scenario, the mean values (across the model domain) of which are plotted for a 4 day period at the end of the campaign in Fig. 13a. Throughout the middle of the day (roughly between 10:00 and 15:00 UTC) the net tendency is an increase in total nitrate mass loading, strongest in the lower atmosphere (peaking at ground level, and extending up to 950–940 hPa) at midday (with domain means reaching 0.25 µg kg$_{\text{air}}^{-1}$ h^{-1}). Over the rest of the day depositional losses of nitrate dominate, with domain mean tendencies dropping below -0.1 µg kg$_{\text{air}}^{-1}$ h^{-1} at ground level in the evening/early-nighttime (before midnight).

During the "het on" scenario daytime nitrate formation still dominates, although the domain mean tendencies are lower, only reaching 0.15 $\mu g\,kg_{air}^{-1}\,h^{-1}$ (Fig. 13b). Losses in the evening and early morning are of a similar magnitude to those in the "het off" scenario, however the domain mean tendencies during the middle of the night are now close to zero. The potential contribution of N_2O_5 heterogeneous chemistry to the total nitrate mass loadings is illustrated in Fig. 13c (this is calculated by taking the integrated uptake rate of N_2O_5, and does not take into consideration the production of $ClNO_2$). This contribution is strongest between 23:00 and 03:00 UTC, with domain mean values between 0.075–0.1 $\mu g\,kg_{air}^{-1}\,h^{-1}$ (similar in magnitude to the increase in tendencies between the "het off" and "het on" scenarios during these same periods).

This offsetting of depositional losses by N_2O_5 heterogeneous chemistry gives rise to the maintenance of higher nitrate aerosol mass loadings during the night. The statistical variation in PM_{10} nitrate mass loadings across the model domain (at 990 hPa) for the "het off" and "het on" scenarios are shown in Fig. 14a and b, respectively. Data from 15 days through the campaign are used (discarding the first 4 days of the model run as spin up, as well as data from the 21 July due to the discontinuity caused by the meteorological restart) to obtain a diurnal cycle representative of the whole campaign period. During the "het off" scenario the maximum PM_{10} nitrate mass loadings occur at around 15:00 and 16:00 UTC (with median and mean mass loadings of 0.8 and 1.6 $\mu g\,kg_{air}^{-1}$, and 95th percentile of 5.6 $\mu g\,kg_{air}^{-1}$), and the minimum PM_{10} nitrate mass loadings occur at around 06:00 UTC (with median and mean mass loadings of 0.3 and 0.9 $\mu g\,kg_{air}^{-1}$, and 95th percentile of 3.5 $\mu g\,kg_{air}^{-1}$). In between these two extremes the PM_{10} mass loadings vary in a smooth, roughly sinusoidal, manner.

During the "het on" scenario the maximum PM_{10} nitrate mass loadings around 15:00 and 16:00 UTC are very similar to those in the "het off" scenario (although there is a small, 1–3 %, decrease), however the PM_{10} nitrate mass loadings at 06:00 UTC have increased dramatically (with median and mean mass loadings of 0.4 and 1.1 $\mu g\,kg_{air}^{-1}$, and 95th percentile of 4.6 $\mu g\,kg_{air}^{-1}$) This is in agreement with the findings of Riemer et al. (2003), who showed that N_2O_5 heterogeneous reactions had a large impact on regional aerosol nitrate fields at night. In the early evening the PM_{10} nitrate mass loadings decrease in a similar manner in both scenarios

– they only begin to diverge around 22:00 UTC. While the reduction in median mass loadings during the night is slowed during the "het on" scenario, the reduction in the 95th percentiles is actually reversed between 22:00 and 02:00 UTC, leading to a secondary peak of 5.0 $\mu g\,kg_{air}^{-1}$ at this time. This indicates that nitrate formation via the N_2O_5 heterogeneous pathway is strongly associated with pollution plumes, in contrast to nitrate formation via the $NO_2 + OH$ pathway which, because it is limited by the abundance of OH and does not directly produce aerosol nitrate (instead producing gas-phase HNO_3 which then condenses onto available non-acidic particles), is a more diffuse process.

Summer-time measurements of nitrate particulate mass across Europe exhibit a very different diurnal profile to these model predictions: the measurements show a steady increase in nitrate mass loadings through the night, reaching the maximum at about 06:00 UTC (around dawn) followed by a sharp drop in nitrate mass loading through the day, to reach a minimum around 18:00 UTC (around sunset) (Poulain et al., 2011). The measured nitrate mass loadings generally show an anti-correlation with temperature, and correlation with RH, leading to the suggestion that the diurnal variation in particulate nitrate is principally driven by changes in the thermodynamic equilibrium of ammonium nitrate. As WRF-Chem is known to under-predict temperature, and over-predict daytime specific humidities, within the PBL (García-Díez et al., 2013) it is, unfortunately, unsurprising that the diurnal cycle in nitrate mass loadings in the model is so different. However Poulain et al. (2011) also used a simplified box-model to examine the potential contribution of N_2O_5 heterogeneous chemistry to particulate nitrate formation; they showed a clear linear relationship between the measured and modelled (potential) particulate nitrate mass loadings, indicating that N_2O_5 heterogeneous chemistry is an important route for particulate nitrate formation (in agreement with previous studies, cf. Chang et al., 2011, and references therein). The results from this study are in agreement with these previous studies: N_2O_5 heterogeneous chemistry is an important source of particulate nitrate, and helps to bring the model diurnal profile closer the measured profiles. This shows that the inclusion of N_2O_5 heterogeneous chemistry is an important step towards the more realistic simulation of nitrate aerosol mass loadings.

The regional influence of the N_2O_5 heterogeneous chemistry on gas-phase chemistry can be investigated using the instantaneous VOC tendencies ($\mathrm{dVOC}/\mathrm{d}t$, $\mathrm{molecules\,cm^{-3}\,s^{-1}}$) with respect to oxidation by OH and NO_3. This tendency for OH is calculated as:

$$\left.\frac{\mathrm{d[VOC]}}{\mathrm{d}t}\right|_{\mathrm{OH}} = -[\mathrm{OH}]\sum_{i=1}^{n}(k_{\mathrm{OH},i}[\mathrm{VOC}]_i), \tag{8}$$

where $k_{\mathrm{OH},i}$ is the reaction rate of VOC_i with OH, and n is the number of VOC's which react with OH. An equivalent equation is used for NO_3, and to investigate the instantaneous DMS tendencies ($\mathrm{dDMS}/\mathrm{d}t$) with respect to OH and NO_3.

The statistical variation in the tendencies for total NMVOCs, Alkenes, and DMS, across the model domain, are shown in Fig. 15a–c, respectively. Campaign-averaged statistics are generated using data from the same 15 days as above – the diurnal cycle and vertical variation in these tendencies are shown in the Supplement, in Fig. 15 only data for midday (12:00 UTC) and midnight (00:00 UTC), and at the 990 hPa pressure level, are plotted.

Daytime reaction with OH dominates the oxidation of NMVOCs (and, more selectively, just Alkenes), with median and mean tendencies of 2.4×10^6 (0.6×10^5) and 4.0×10^6 (6.0×10^5) $\mathrm{molecules\,cm^{-3}\,s^{-1}}$, respectively. The OH oxidation of NMVOCs is not particularly homogeneous across the domain, the 75th percentile is $\times 5$ greater than the 25th percentile, however for Alkenes this process is even more strongly concentrated in the pollution plumes, the 75th percentile being $\times 50$ greater than the 25th percentile.

At night NO_3 oxidation is more important than OH oxidation for NMVOCs, with median and mean rates for NO_3 $\times$ 4–5 greater than those for OH. However these rates are still $\times$ 100–300 lower than the daytime OH oxidation rates, and strongly constrained to the pollution plumes. This is especially marked for the oxidation of Alkenes by NO_3, for which the median values are $\times$ 80 lower than those for daytime OH oxidation, while the 95th percentiles are only $\times$ 8 lower. N_2O_5 heterogeneous chemistry suppresses NO_3 concentrations, and so reduces nighttime NO_3 oxidation, as well as nightime OH oxidation (due to the principal source of nighttime OH being NO_3 oxidation). The magnitude of this suppression is small though, generally a factor of 1.5 or less.

Nighttime NO_3 oxidation of DMS is more important than daytime OH oxidation, with median and mean tendencies of 2.8×10^4 and 4.5×10^4 molecules cm^{-3} s^{-1} for NO_3, compared with 2.2×10^4 and 3.1×10^4 molecules cm^{-3} s^{-1} for OH. Suppressing NO_3 concentrations via N_2O_5 heterogeneous chemistry reduces the NO_3 oxidation rates within pollution plumes (reducing the 95th percentile from 1.6×10^5 to 1.4×10^5 molecules cm^{-3} s^{-1}), allowing greater regional diffusion of DMS leading to (small) increases in the background NO_3 and OH oxidation rates.

4 Conclusions

As part of the RONOCO project comparisons have been made between measurements and a detailed regional model (WRF-Chem). It has been demonstrated that N_2O_5 heterogeneous chemistry on aqueous aerosol droplets is an important process for controlling the NO_3 and N_2O_5 mixing ratios over N–W Europe. However the impact of this process is strongly dependent on the aerosol water content, which is very sensitive to atmospheric relative humidity. Above 70–75 % RH this process strongly limits build up of NO_3 and N_2O_5, and can be very efficient in converting NO_x to NO_z . At relative humidities of 60–70 % or lower N_2O_5 heterogeneous chemistry becomes very inefficient, essentially switching it off. For regional modelling purposes it is essential to properly reproduce the atmospheric relative humidity, failure to do so will lead to erroneous estimates of N_2O_5 heterogeneous chemical rates. Similarly, the transport of chemical species is very dependent on the meteorological fields and parameterisations of the model. The biases in temperature, specific humidity, and PBL stability within WRF (García-Díez et al., 2013; Krogæter and Reuder, 2014) have negatively impacted on the WRF-Chem results presented here and in previous studies (McKeen et al., 2007). Correcting these biases in WRF will significantly improve the model skill of WRF-Chem.

The dependence of N_2O_5 heterogeneous chemistry on aerosol particle composition is complex. The model skill at accurately predicting aerosol composition is a lot lower than its skill in replicating the gas-phase chemistry. More work is required to remedy this shortfall (particularly with regards to the under-prediction of ammonium-sulphate aerosol). To help constrain

this model development, it would be useful to have more widespread measurements of the composition of supra-micron aerosol particles, as well as gas-phase NH_3, as a complement to the AMS measurements.

NO_3 is the main oxidant during the nighttime, the mean reaction rate with VOC's being $\times$ 4–5 greater than that for OH. However this is $\times$ 100–300 slower than the mean reaction rate of OH with VOC's during the day, and it is far more spatially heterogeneous process, principally confined to the more polluted regions of the domain. Only for the oxidation of DMS is the contribution of NO_3 on a par with that of OH. By limiting the build-up of NO_3, N_2O_5 heterogeneous processing does reduce the oxidative capacity of the atmosphere a little. However its impact on the overall oxidative capacity of the atmosphere is insignificant.

N_2O_5 heterogeneous chemistry is an important process with regards to the regional aerosol nitrate budget – by providing an alternative pathway for converting NO_x emissions to aerosol nitrate, which operates during the periods at which HNO_3 formation by the $NO_2 + OH$ pathway is smallest. This substantially contributes to nitrate aerosol mass loadings through the nighttime, and so will increase the negative impact that NO_x emissions have on air quality over N–W Europe. However, the model skill at reproducing the summer diurnal cycle of nitrate aerosol mass loadings across N–W Europe is poor, due at least in part to the systematic biases in meteorological fields noted above. Correcting these biases will enable better modelling of regional particulate matter distributions, and so improve our understanding of the impact of this on European air quality.

The Supplement related to this article is available online at doi:10.5194/acpd-0-1-2014-supplement.

Acknowledgements. We would like to acknowledge the efforts of the whole RONOCO team during and after the project. Airborne data was obtained using the BAe-146-301 Atmospheric Research Aircraft (ARA) flown by Directflight Ltd and managed by the Facility for Airborne Atmospheric Measurements (FAAM), which is a joint entity of the Natural Environment Research Council (NERC) and the Met Office. The NERC National Centre for Atmospheric Science (NCAS) Atmospheric Measurement Facility

(AMF) supported the maintenance of the cToF-AMS. NCAS also supported the development of the data interpretation methods employed here through its Composition Directorate. This work was supported by the NERC RONOCO project NE/F004656/1. S. Archer-Nicholls was supported by a Nature Environment Research Council (NERC) quota studentship. Model runs were carried out on the High End Computing Terascale Resources (HECToR) British national supercomputer.

References

Abdul-Razzak, H. and S. J. Ghan: A parameterisation of aerosol activation: 3. Sectional representation, J. Geophys. Res., 107, 4026, doi:10.1029/2001JD000483, 2002.

Allan, B. J., McFiggans, G., Plane, J. M. C., Coe, H., and McFadyen, G. G.: The nitrate radical in the remote marine boundary layer, J. Geophys. Res., 105, 24191–24204, doi:10.1029/2000JD900314, 2000.

Anttila, T., Kiendler-Scharr, A., Tillmann, R., and Mentel, T. F.: On the reactive uptake of gaseous compounds by organic-coated aqueous aerosols: theoretical analysis and application to the heterogeneous hydrolysis of N_2O_5, J. Phys. Chem. A, 110, 10435–10443, 2006.

Archer-Nicholls, S., Lowe, D., Utembe, S., Allan, J., Zaveri, R. A., Fast, J. D., Hodnebrog, Ø., Denier van der Gon, H., and McFiggans, G.: Gaseous chemistry and aerosol mechanism developments for version 3.5.1 of the online regional model, WRF-Chem, Geosci. Model Dev. Discuss., 7, 871–929, doi:10.5194/gmdd-7-871-2014, 2014.

Asaf, D., Tas, E., Pedersen, D., Peleg, M., and Luria, M.: Long-term measurements of NO_3 radical at a semiarid urban site: 2. Seasonal trends and loss mechanisms, Environ. Sci. Technol., 44, 5001–5007, doi:10.1021/es100967z, 2010.

Atkinson, R.: Atmospheric chemistry of VOCs and NO_x, Atmos. Environ., 34, 2063–2101, doi:10.1016/S1352-2310(99)00460-4, 2000.

Atkinson, R. and Arey, J.: Atmospheric degradation of volatile organic compounds, Chem. Rev., 103, 4605–4638, doi:10.1021/cr0206420, 2003.

Atkinson, R., Baulch, D. L., Cox, R. A., Crowley, J. N., Hampson, R. F., Hynes, R. G., Jenkin, M. E., Rossi, M. J., and Troe, J.: Evaluated kinetic and photochemical data for atmospheric chemistry: Volume I – gas phase reactions of O_x, HO_x, NO_x and SO_x species, Atmos. Chem. Phys., 4, 1461–1738, doi:10.5194/acp-4-1461-2004, 2004.

Bahreini, R., Ervens, B., Middlebrook, A. M., Warneke, C., de Gouw, J. A., DeCarlo, P. F., Jimenez, J. L., Brock, C. A., Neuman, J. A., Ryerson, T. B., Stark, H., Atlas, E., Brioude, J., Fried, A., Holloway, J. S., Peischl, J., Richter, D., Walega, J., Weibring, P., Wollny, A. G., and Fehsenfeld, F. C.: Organic aerosol formation in urban and industrial plumes near Houston and Dallas, Texas, J. Geophys. Res., 114, D00F16, doi:10.1029/2008JD011493, 2009.

Bertram, T. H. and Thornton, J. A.: Toward a general parameterization of N_2O_5 reactivity on aqueous particles: the competing effects of particle liquid water, nitrate and chloride, Atmos. Chem. Phys., 9, 8351–8363, doi:10.5194/acp-9-8351-2009, 2009.

Brown, S. S. and Stutz, J.: nighttime radical observations and chemistry, Chem. Soc. Rev., 41, 6405–6447, doi:10.1039/c2cs35181a, 2012.

Brown, S. S., Ryerson, T. B., Wollny, A. G., Brock, C. A., Peltier, R., Sullivan, A. P., Weber, R. J., Dubé, W. P., Trainer, M., Meagher, J. F., Fehsenfeld, F. C., and Ravishankara, A. R.: Variability in nocturnal nitrogen oxide processing and its role in regional air quality, Science, 311, 67–70, doi:10.1126/science.1120120, 2006.

Brown, S. S., Dubé, W. P., Fuchs, H., Ryerson, T. B., Wollny, A. G., Brock, C. A., Bahreini, R., Middlebrook, A. M., Neuman, J. A., Atlas, E., Roberts, J. M., Ostoff, H. D., Trainer, M., Fehsenfeld, F. C., and Ravishankara, A. R.: Reactive uptake coefficients for N_2O_5 determined from aircraft measurements during the Second Texas Air Quality Study: comparison to current model parameterizations, J. Geophys. Res., 114, D00F10, doi:10.1029/2008JD011679, 2009.

Butkovskaya, N. I. and LeBras, G.: mechanism of the $NO_3 + DMS$ reaction by discharge flow mass spectrometry, J. Phys. Chem., 98, 2582–2591, doi:10.1021/j100061a014, 1994.

Canagaratna, M. R., Jayne, J. T., Jimenez, J. L., Allan, J. D., Alfarra, M. R., Zhang, Q., Onasch, T. B., Drewnick, F., Coe, H., Middlebrook, A., Delia, A., Williams, L. R., Trimborn, A. M., Northway, M. J., DeCarlo, P. F., Kolb, C. E., Davidovits, P., and Worsnop, D. R.: Chemical and microphysical characterization of ambient aerosols with the aerodyne aerosol mass spectrometer, Mass Spectrom. Rev., 26, 185–222, 635, doi:10.1002/mas.20115, 2007.

Chang, W. L., Bhave, P. V., Brown, S. S., Riemer, N., Stutz, J. and Dabdub, D.: Heterogeneous atmospheric chemistry, ambient measurements, and model calculations of N_2O_5: a review, Aerosol Sci. Tech., 45, 665–695, doi:10.1080/02786826.2010.551672, 2011.

Chou, M.-D. and Suarez, M. J.: An Efficient Thermal Infrared Radiation Parameterization for Use in General Circulation Models, NASA Tech. Memo. 104606, 85 pp., 1994.

Davis, J. M., Bhave, P. V., and Foley, K. M.: Parameterization of N_2O_5 reaction probabilities on the surface of particles containing ammonium, sulfate, and nitrate, Atmos. Chem. Phys., 8, 5295–5311, doi:10.5194/acp-8-5295-2008, 2008.

Dee, D. P., Uppala, S. M., Simmons, A. J., Berrisford, P., Poli, P., Kobayashi, S., Andrae, U., Balmaseda, M. A., Balsamo, G., Bauer, P., Bechtold, P., Beljaars, A. C. M., van de Berg, L., Bidlot, J., Bormann, N., Delsol, C., Dragani, R., Fuentes, M., Geer, A. J., Haimberger, L., Healy, S. B., Hersbach, H., Hólm, E. V., Isaksen, L., Kållberg, P., Köhler, M., Matricardi, M., McNally, A. P., Monge-Sanz, B. M., Morcrette, J.-J., Park, B.-K., Peubey, C., de Rosnay, P., Tavolato, C., Thépaut, J.-N., and Vitart, F.: The ERA-interim reanalysis: configuration and performance of the data assimilation system, Q. J. Roy. Meteor. Soc., 137, 553–597, doi:10.1002/qj.828, 2011.

DeMore, W. B., Sander, S. P., Howard, C. J., Ravishankara, A. R., Golden, D. M., Kolb, C. E., Hampson, R. F., Kurylo, M. J., Molina, M. J.: Chemical kinetics and photochemical data for use in stratospheric modeling, Eval. 11. NASA Jet Propul. Lab., Calif. Inst. of Technol., Pasadena, 1994.

Denier van der Gon, H. A. C., Visschedijk, A., van der Brugh, H., and Dröge, R.: A High Resolution European Emission Data Base for the Year 2005, a Contribution to UBA – Projekt PAREST: Particle Reduction Strategies, TNO report TNO-034-UT-2010-01895_RPT-ML, Utrecht, 2010.

Dentener, F. J. and Crutzen, P. J.: Reaction of N_20_5 on tropospheric aerosols: impact on the global distributions of NO_x, 0_3, and OH, J. Geophys. Res., 98, 7149–7163, 1993.

Di Carlo, P., Aruffo, E., Busilacchio, M., Giammaria, F., Dari-Salisburgo, C., Biancofiore, F., Visconti, G., Lee, J., Moller, S., Reeves, C. E., Bauguitte, S., Forster, G., Jones, R. L., and Ouyang, B.: Aircraft based four-channel thermal dissociation laser induced fluorescence instrument for simultaneous measurements of NO_2, total peroxy nitrate, total alkyl nitrate, and HNO_3, Atmos. Meas. Tech., 6, 971–980, doi:10.5194/amt-6-971-2013, 2013.

Drewnick, F., Hings, S. S., DeCarlo, P., Jayne, J. T., Gonin, M., Fuhrer, K., Weimer, S., Jimenez, J. L., Demerjian, K. L., Borrmann, S., and Worsnop, D. R.: A new Time-of-Flight Aerosol Mass Spectrometer (TOF-655 AMS) instrument description and first field deployment, Aerosol Sci. Tech., 39, 637–658, doi:10.1080/02786820500182040, 2005.

Ek, M. B., Mitchell, K. E., Lin, Y., Rogers, E., Grunmann, P., Koren, V., Gayno, G., and Tarpley, J. D.: Implementation of Noah land surface model advances in the National Centers for Environmental Prediction operational mesoscale Eta model, J. Geophys. Res., 10, 8851, doi:10.1029/2002JD003296, 2003.

Emmons, L. K., Walters, S., Hess, P. G., Lamarque, J.-F., Pfister, G. G., Fillmore, D., Granier, C., Guenther, A., Kinnison, D., Laepple, T., Orlando, J., Tie, X., Tyndall, G., Wiedinmyer, C., Baughcum, S. L.,

and Kloster, S.: Description and evaluation of the Model for Ozone and Related chemical Tracers, version 4 (MOZART-4), Geosci. Model Dev., 3, 43–67, doi:10.5194/gmd-3-43-2010, 2010.

Fehsenfeld, F. C., Ancellet, G., Bates, T. S., Goldstein, A. H., Hardesty, R. M., Honrath, R., Law, K. S., Lewis, A. C., Leaitch, R., McKeen, S., Meagher, J., Parrish, D. D., Pszenny, A. A. P., Russell, P. B., Schlager, H., Seinfeld, J., Talbot, R., and Zbinden, R.: International Consortium for Atmospheric Research on Transport and Transformation (ICARTT): North America to Europe – overview of the 2004 summer field study, J. Geophys. Res., 111, D23, doi:10.1029/2006JD007829, 2006.

Fuentes, E., Coe, H., Green, D., and McFiggans, G.: On the impacts of phytoplankton-derived organic matter on the properties of the primary marine aerosol – Part 2: Composition, hygroscopicity and cloud condensation activity, Atmos. Chem. Phys., 11, 2585–2602, doi:10.5194/acp-11-2585-2011, 2011.

García-Díez, M., Fernández, J., Fita, L., and Yagüe, C.: Seasonal dependence of WRF model biases and sensitivity to PBL schemes over Europe, Q. J. Roy. Meteor. Soc., 139, 501–514, doi:10.1002/qj.1976, 2013

Gong, S. L., Bartie, L. A., and Blanchet, J.-P.: Modeling sea-salt aerosols in the atmosphere 1. Model development, J. Geophys. Res., 102, 3805–3818, 1997.

Grell, G. A., Peckham, S. E., Schmitz, R., McKeen, S. A., Frost, G., Skamarock, W. C. and Eder, B.: Fully coupled "online" chemistry within the WRF model, Atmos. Environ., 39, 6957–6975, doi:10.1016/j.atmosenv.2005.04.027, 2005.

Guenther, A., Karl, T., Harley, P., Wiedinmyer, C., Palmer, P. I., and Geron, C.: Estimates of global terrestrial isoprene emissions using MEGAN (Model of Emissions of Gases and Aerosols from Nature), Atmos. Chem. Phys., 6, 3181–3210, doi:10.5194/acp-6-3181-2006, 2006.

Heikes, B. G. and Thompson, A. M.: Effects of heterogeneous processes on NO_3, HONO, and HNO_3 chemistry in the troposphere, J. Geophys. Res., 88, 10883–10895, doi:10.1029/JC088iC15p10883, 1983.

Hoyle, C. R., Boy, M., Donahue, N. M., Fry, J. L., Glasius, M., Guenther, A., Hallar, A. G., Huff Hartz, K., Petters, M. D., Petäjä, T., Rosenoern, T., and Sullivan, A. P.: A review of the anthropogenic influence on biogenic secondary organic aerosol, Atmos. Chem. Phys., 11, 321–343, doi:10.5194/acp-11-321-2011, 2011.

Inness, A., Baier, F., Benedetti, A., Bouarar, I., Chabrillat, S., Clark, H., Clerbaux, C., Coheur, P., Engelen, R. J., Errera, Q., Flemming, J., George, M., Granier, C., Hadji-Lazaro, J., Huijnen, V., Hurtmans, D., Jones, L., Kaiser, J. W., Kapsomenakis, J., Lefever, K., Leitão, J., Razinger, M., Richter, A., Schultz, M. G., Simmons, A. J., Suttie, M., Stein, O., Thépaut, J.-N., Thouret, V., Vrekoussis, M.,

Zerefos, C., and the MACC team: The MACC reanalysis: an 8 yr data set of atmospheric composition, Atmos. Chem. Phys., 13, 4073–4109, doi:10.5194/acp-13-4073-2013, 2013.

Janjic., Z. I.: The step-mountain coordinate: physical package, Mon. Weather Rev., 118, 1429–1443, 1990.

Janjic., Z. I.: The step-mountain eta coordinate model: further developments of the convection, viscous sublayer, and turbulence closure schemes, Mon. Weather Rev., 122, 927–945, 1994.

Jenkin, M. E., Watson, L. A., Utembe, S. R., and Shallcross, D. E.: A Common Representative Intermediates (CRI) mechanism for VOC degradation. Part 1: Gas phase mechanism development, Atmos. Environ., 42, 7185–7195, doi:10.1016/j.atmosenv.2008.07.028, 2008.

John, W., Wall, S. M., Ondo, J. L., and Winklmayr, W.: Modes in the size distribution of atmospheric inorganic aerosol, Atmos. Environ., 24A, 2349–2359, 1990.

Kennedy, O. J., Ouyang, B., Kennedy, O. J., Ouyang, B., Langridge, J. M., Daniels, M. J. S., Bauguitte, S., Freshwater, R., McLeod, M. W., Ironmonger, C., Sendall, J., Norris, O., Nightingale, R., Ball, S. M., and Jones, R. L.: An aircraft based three channel broadband cavity enhanced absorption spectrometer for simultaneous measurements of NO_3, N_2O_5 and NO_2, Atmos. Meas. Tech., 4, 1759–1776, doi:10.5194/amt-4-1759-2011, 2011.

Kettle, A. J., Andreae, M. O., Amouroux, D., Andreae, T. W., Bates, T. S., Berresheim, H., Bingemer, H., Boniforti, R., Curran, M. A. J., DiTullio, G. R., Helas, G., Jones, G. B., Keller, M. D., Kiene, R. P., Leck, C., Levasseur, M., Malin, G., Maspero, M., Matrai, P., McTaggart, A. R., Mihalopoulos, N., Nguyen, B. C., Novo, A., Putaud, J. P., Rapsomanikis, S., Roberts, G., Schebeske, G., Sharma, S., Simó, R., Staubes, R., Turner, S., and Uher, G.: A global database of sea surface dimethylsulfide (DMS) measurements and a procedure to predict sea surface DMS as a function of latitude, longitude, and month, Global Biogeochem. Cy., 13, 399–444, 1999.

Krogæter, O. and Reuder, J.: Validation of boundary layer parameterization schemes in the Weather Research and Forecasting (WRF) model under the aspect of offshore wind energy applications – Part II: Boundary layer height and atmospheric stability, Wind Energ., doi:10.1002/we.1765, 2014

Le Breton, M., McGillen, M. R., Muller, J. B. A., Bacak, A., Shallcross, D. E., Xiao, P., Huey, L. G., Tanner, D., Coe, H., and Percival, C. J.: Airborne observations of formic acid using a chemical ionization mass spectrometer, Atmos. Meas. Tech., 5, 3029–3039, doi:10.5194/amt-5-3029-2012, 2012.

Le Breton, M., Bacak, A, Muller, J. B. A., Xiao, P., Shallcross, B. M. A., Batt, R., Cooke, M. C., Shallcross, D. E., Bauguitte, S. J.-B., and Percival, C. J.: Simultaneous airborne nitric acid and formic acid measurements using a chemical ionization mass spectrometer around the UK: analysis of primary and

secondary production pathways, Atmos. Environ., 83, 166–175, doi:10.1016/j.atmosenv.2013.10.008, 2013.

Li, S.-M., Anlauf, K. G., and Wiebe, H. A.: Heterogeneous nighttime production and deposition of particle nitrate at a rural site in North America during summer 1988, J. Geophys. Res., 98, 5139–5157, 1993.

Lin, Y.-L., Farley, R. D., and Orville, H. D.: Bulk parameterisation of the snow field in a cloud model, J. Clim. Appl. Meteorol., 22, 1065–1092, 1983

McKeen, S., Chung, S. H., Wilczak, J., Grell, G., Djalalova, I., Peckham, S., Gong, W., Bouchet, V., Moffet, R., Tang, Y., Carmichael, G. R., Mathur, R., and Yu, S.: Evaluation of several $PM_{2.5}$ forecast models using data collected during the ICARTT/NEAQS 2004 field study, J. Geophys. Res., 112, D10S20, doi:10.1029/2006JD007608, 2007.

Mellor, G. L. and Yamada, T.: A hierarchy of turbulence closure models for planetary boundary layers, J. Atmos. Sci., 31, 1791–1806, 1974.

Mlawer, E. J., Taubman, S. J., Brown, P. D., Iacono, M. J., and Clough, S. A.: Radiative transfer for inhomogeneous atmospheres: RRTM, a validated correlated-k model for the longwave, J. Geophys. Res., 102, 16663–16682, 1997.

Morgan, W. T., Ouyang, B., Allan, J. D., Aruffo, E., Di Carlo, P., Kennedy, O. J., Lowe, D., Flynn, M. J., Rosenberg, P. D., Williams, P. I., Jones, R., McFiggans, G. B., and Coe, H.: Influence of aerosol chemical composition on N_2O_5 uptake: airborne regional measurements in North-Western Europe, Atmos. Chem. Phys. Discuss., 14, 19673–19718, doi:10.5194/acpd-14-19673-2014, 2014.

Neusüß, C., Wex, H., Birmili, W., Wiedensohler, A., Koziar, C., Busch, B., Brüggemann, E., Gnauk, T., Ebert, M., and Covert, D. S.: Characterization and parameterization of atmospheric particle number-, mass-, and chemical-size distributions in central Europe during LACE 98 and MINT, J. Geophys. Res., 107, 8127, doi:10.1029/2001JD000514, 2002.

Nowak, J. B., Neuman, J. A., Kozai, K., Huey, L. G., Tanner, D. J., Holloway, J. S., Ryerson, T. B., Frost, G. J., McKeen, S. A., and Fehsenfeld, F. C.: A chemical ionization mass spectrometry technique for airborne measurements of ammonia, J. Geophys. Res., 112, D10S02, doi:10.1029/2006JD007589, 2007.

Osthoff, H. D., Pilling, M. J., Ravishankara, A. R., and Brown, S. S.: Temperature dependence of the NO_3 absorption cross-section above 298 K and determination of the equilibrium constant for $NO_3 + NO_2 \leftrightarrow N_2O_5$ at atmospherically relevant conditions, Phys. Chem. Chem. Phys., 9, 5785–5793, doi:10.1039/b709193a, 2007.

Platt, U. and Le Bras, G.: Influence of DMS on the O_x-NO_y partitioning and the NO_x distribution in the marine background atmosphere, Geophys. Res. Lett., 24, 1935–1938, 1997.

Poulain, L., Spindler, G., Birmili, W., Plass-Dülmer, C., Wiedensohler, A., and Herrmann, H.: Seasonal and diurnal variations of particulate nitrate and organic matter at the IfT research station Melpitz, Atmos. Chem. Phys., 11, 12579–12599, doi:10.5194/acp-11-12579-2011, 2011.

Putaud, J.-P., Raes, F., Van Dingenen, R., Brüggemann, E., Facchini, M.-C., Decesari, S., Fuzzi, S., Gehrig, R., Hüglin, C., Laj, P., Lorbeer, G., Maenhaut, W., Mihalopoulos, N., Müller, K., Querol, X., Rodriguez, S., Schneider, J., Spindler, G., ten Brink, H., Tørseth, K., and Wiedensohler, A.: A European aerosol phenomenology – 2: Chemical characteristics of particulate matter at kerbside, urban, rural and background sites in Europe, Atmos. Environ., 38, 2579–2595, doi:10.1016/j.atmosenv.2004.01.041, 2004.

Riemer, N., Vogel, H., Vogel, B., Schell, B., Ackermann, I., Kessler, C., and Hass, H.: Impact of the heterogeneous hydrolysis of N_2O_5 on chemistry and nitrate aerosol formation in the lower troposphere under photosmog conditions, J. Geophys. Res., 108, 4144, doi:10.1029/2002JD002436, 2003.

Riemer, N., Vogel, H., Vogel, B., Anttila, T., Kiendler-Scharr, A. and Mentel, T. F.: Relative importance of organic coatings for the heterogeneous hydrolysis of N_2O_5 during summer in Europe, J. Geophys. Res., 114, D17307, doi:10.1029/2008JD011369, 2009.

Sakulyanontvittaya, T., Duhl, T., Wiedinmyer, C., Helmig, D., Matsunaga, S., Potosnak, M., Milford, J., and Guenther, A.: Monoterpene and sesquiterpene emission estimates for the United States, Environ. Sci. Technol., 42, 1623–1629, doi:10.1021/es702274e, 2008.

Slusher, D. L., Huey, L. G., Tanner, D. J., Flocke, F. M., and Roberts, J. M.: A thermal dissociation-chemical ionization mass spectrometry (td-cims) technique for the simultaneous measurement of peroxyacyl nitrates and dinitrogen pentoxide, J. Geophys. Res., 109, D19315, doi:10.1029/2004JD004670, 2004.

Stein, O., Flemming, J., Inness, A., and Kaiser, J. W.: Global reactive gases forecasts and reanalysis in the MACC project, Journal of Integrative Environmental Sciences, 9, 1–14, doi:10.1080/1943815X.2012.696545, 2012.

Taylor, K. E.: Summarizing multiple aspects of model performance in a single diagram, J. Geophys. Res., 106, 7183–7192, doi:10.1029/2000JD900719, 2001.

Thornton, J. A., Kercher, J. P., Riedel, T. P., Wagner, N. L., Cozic, J., Holloway, J. S., Dubé, W. P., Wolfe, G. M., Quinn, P. K., Middlebrook, A. M., Alexander, B., and Brown, S. S.: A large atomic chlorine source inferred from mid-continental reactive nitrogen chemistry, Nature, 464, 7286, 271–274, doi:10.1038/nature08905, 2010.

Utembe, S. R., Watson, L. A., Shallcross, D. E., and Jenkin, M. E.: A Common Representative Intermediates (CRI) mechanism for VOC degradation. Part 3: Development of a secondary organic aerosol module, Atmos. Environ., 43, 1982–1990, doi:10.1016/j.atmosenv.2009.01.008, 2009.

von Glasow, R. and Crutzen, P. J.: Model study of multiphase DMS oxidation with a focus on halogens, Atmos. Chem. Phys., 4, 589–608, doi:10.5194/acp-4-589-2004, 2004.

Wall, S. M., John, W., and Ondo, J. L.: Measurement of aerosol size distributions for nitrate and major ionic species, Atmos. Environ., 22, 1649–1656, 1988.

Watson, L. A., Shallcross, D. E., Utembe, S. R., and Jenkin, M. E.: A Common Representative Intermediates (CRI) mechanism for VOC degradation. Part 2: Gas phase mechanism reduction, Atmos. Environ., 42, 7196–7204, doi:10.1016/j.atmosenv.2008.07.034, 2008.

Winer, A. M., Atkinson, R., and Pitts Jr., J. N.: Gaseous nitrate radical: possible nighttime atmospheric sink for biogenic organic compounds, Science, 224, 156–159, 1984.

Zaveri, R. A., Easter, R. C., Fast, J. D., and Peters, L. K.: Model for Simulating Aerosol Interactions and Chemistry (MOSAIC), J. Geophys. Res., 113, D13204, doi:10.1029/2007JD008782, 2008.

Zaveri, R. A., Berkowitz, C. M., Brechtel, F. J., Gilles, M. K., Hubbe, J. M., Jayne, J. T., Kleinman, L. I., Laskin, A., Madronich, S., Onasch, T. B., Pekour, M. S., Springston, S. R., Thornton, J. A., Tivanski, A. V., and Worsnop, D. R.: Nighttime chemical evolution of aerosol and trace gases in a power plant plume: implications for secondary organic nitrate and organosulfate aerosol formation, NO_3 radical chemistry, and N_2O_5 heterogeneous hydrolysis, J. Geophys. Res., 115, D12304, doi:10.1029/2009JD013250, 2010a.

Zaveri, R. A., Voss, P. B., Berkowitz, C. M., Fortner, E., Zheng, J., Zhang, R., Valente, R. J., Tanner, R. L., Holcomb, D., Hartley, T. P., and Baran, L.: Overnight atmospheric transport and chemical processing of photochemically aged Houston urban and petrochemical industrial plume, J. Geophys. Res., 115, D23303, doi:10.1029/2009JD013495, 2010b.

Table 1. Summary of measurements used in this study. Acronyms used are as follows: cToF-AMS (compact Time-of-Flight Aerosol Mass Spectrometer), BBCEAS (BroadBand Cavity Enhanced Absorption Spectrometer), CIMS (Chemical Ionization Mass Spectrometer), and TD-LIF (Thermal Dissociation Laser Induced-Fluorescence).

Measurement	Instrument	Accuracy or Uncertainty
Sub-Micron (0.05–0.8 μm particle diameter) Aerosol Composition	cToF-AMS	30 % (see Bahreini et al., 2009)
N_2O_5	BBCEAS	15 % (Kennedy et al., 2011)
NO_3	BBCEAS	11 % (Kennedy et al., 2011)
HNO_3	CIMS	10 % (Le Breton et al., 2013)
NO_2	TD-LIF	10 % (Di Carlo et al., 2013)
O_3	Ozone Analyser	3 ppb for mixing ratios below 100 ppb

Table 2. Physical parameterisations used in the WRF-Chem model.

Process	WRF-Chem Option	Reference
Microphysics	Lin et al. scheme	Lin et al. (1983); Abdul-Razzak and Ghan (2002)
Cumulus Parameterisation	Grell 3-D ensemble scheme	
Surface Layer	Eta Monin–Obukhov (Janjic) scheme	Janjic (1990, 1994)
Land-surface Model	Unified Noah land-surface model	Ek et al. (2003)
Landuse dataset	USGS	
Planetary boundary layer	Mellor–Yamada–Janjic (MJY) TKE scheme	Mellor and Yamada (1974); Janjic (1990, 1994)
Longwave radiation	RRTMG scheme	Mlawer et al. (1997)
Shortwave radiation	Goddard scheme	Chou and Suarez (1994)

Table 3. Model scenarios.

Scenario	Description
het on	Full inorganic N_2O_5 heterogeneous chemistry following Bertram and Thornton (2009).
no Cl pathway	Inorganic N_2O_5 heterogeneous chemistry, following Bertram and Thornton (2009), but without the Cl^- reactive pathway. All N_2O_5 heterogeneous chemistry now involves H_2O, producing only NO_3^- ions (no $ClNO_2$ products).
organic suppression	Full inorganic N_2O_5 heterogeneous scheme (following Bertram and Thornton, 2009), with organic suppression of uptake following Riemer et al. (2009).

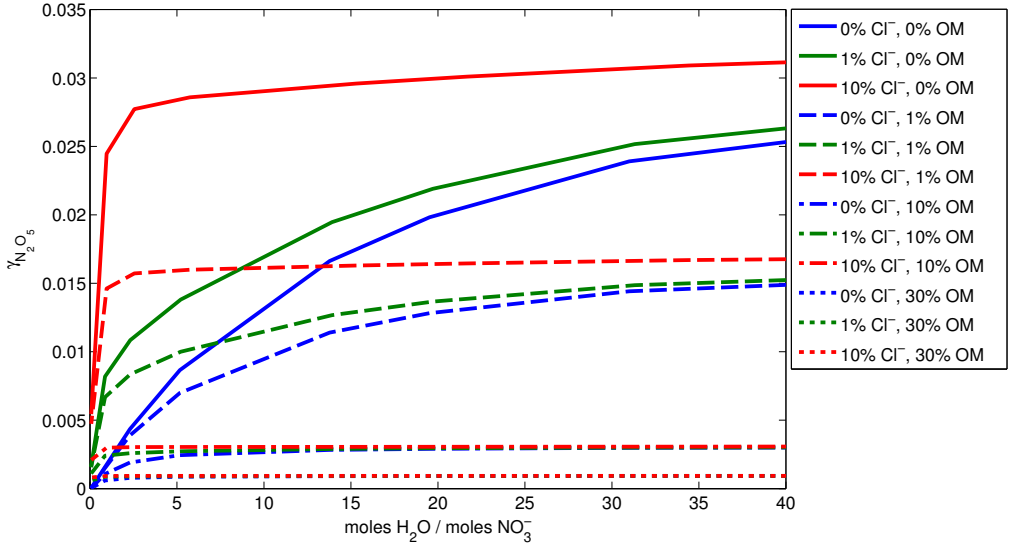

Figure 1. The composition dependence of $\gamma_{N_2O_5}$ for a 1 μm diameter particle, using the inorganic parameterisation of Bertram and Thornton (2009) combined with the organic coating parameterisation of Riemer et al. (2009) . For a range of H_2O:NO_3^- mole ratios, the $\gamma_{N_2O_5}$ for totally inorganic particles with a mole content of chloride ions of 0%, 1%, and 10% are represented by the solid blue, green and red lines, respectively. The suppression of $\gamma_{N_2O_5}$ for these different inorganic particle compositions by an organic shell comprising 1%, 10%, and 30% of the total particle mass are indicated by the dashed, dash-dotted, and dotted lines, respectively.

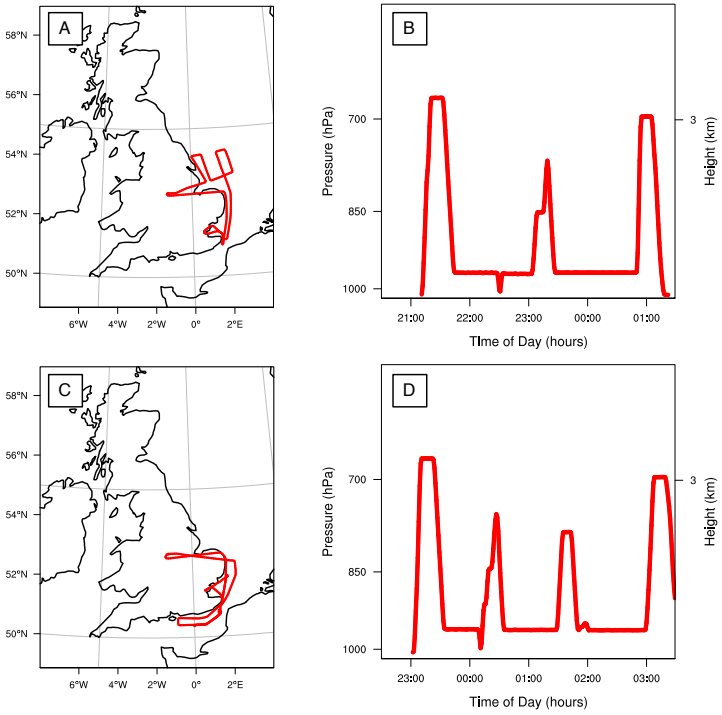

Figure 2. B535 and B541 flight paths (**a** and **c**, respectively) and vertical profiles (**b** and **d**, respectively).

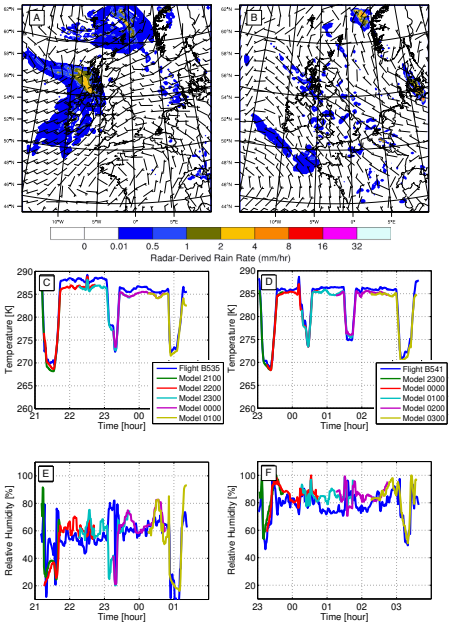

Figure 3. Meteorological fields for flights B535 (**a**, **c**, and **e**) and B541 (**b**, **d**, and **f**). (**a** and **b**) show the simulated radar-derived rainfall rates (and wind fields at 960 hPa) from the model, at 00:00 UTC on the 18 July and 00:00 UTC on the 29 July respectively. (**c** and **d**) compare measured (blue lines) and modelled (multi-coloured lines) air temperature along the flight paths of B535 and B541, respectively. Modelled data is extracted from hourly output files – see main text for details. (**e** and **f**) compare measured and modelled relative humidity along the flight paths of B535 and B541, respectively.

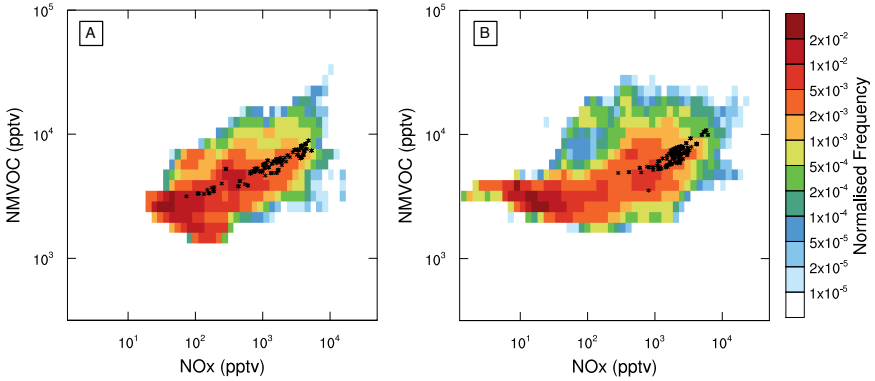

Figure 4. Two-dimensional histogram illustrating the NMVOC : NO_x chemical space across the model domain (at 960 hPa pressure level) during the periods of flights B535 **(a)** and B541 **(b)**. Data frequency is normalised to the total number of grid cells sampled. Model data extracted along the flight tracks are represented by black stars.

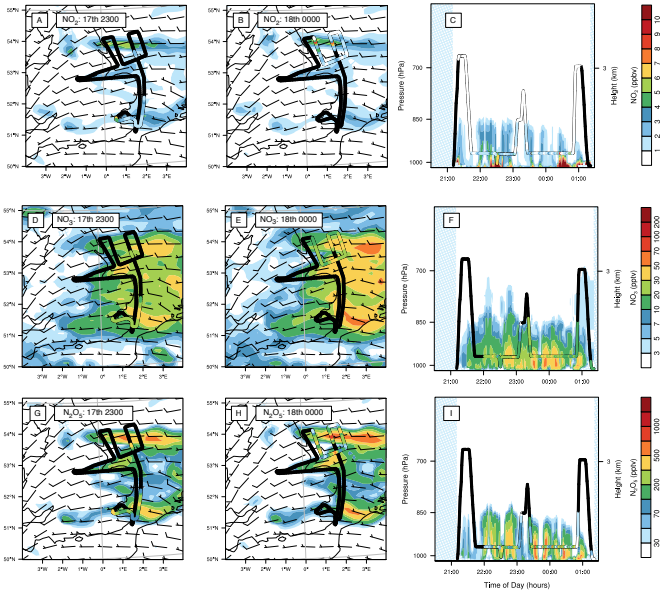

Figure 5. Comparison of NO_2 **(a–c)**, NO_3 **(d–f)** and N_2O_5 **(g–i)** measurements with regional model fields (from the "het on" scenario) for the B535 flight. (**a** and **b**), (**d** and **e**), and (**g** and **h**) show model fields interpolated to 970 hPa at the times indicated in each panel, compared with measurements which are made within $\pm$30 min of that time, and within $\pm$10 hPa of the interpolated model pressure level. (**c**, **f**, and **i**) show the vertical distribution of the model fields along the flight path (extracted $\pm$30 min either side of each output time), with measurement data along the flight path. See the main text for full description.

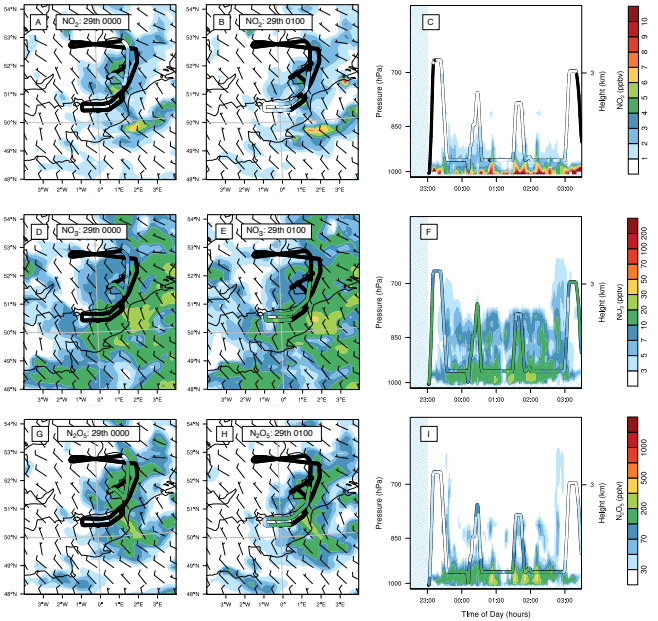

Figure 6. Comparison of NO_2 **(a–c)**, NO_3 **(d–f)** and N_2O_5 **(g–i)** measurements with regional model fields (from the "het on" scenario) for the B541 flight. (**a** and **b**), (**d** and **e**), and (**g** and **h**) show model fields interpolated to 960 hPa at the times indicated in each panel, compared with measurements which are made within $\pm$30 min of that time, and within $\pm$10 hPa of the interpolated model pressure level. (**c**, **f**, and **i**) show the vertical distribution of the model fields along the flight path (extracted $\pm$30 min either side of each output time), with measurement data along the flight path. See the main text for full description.

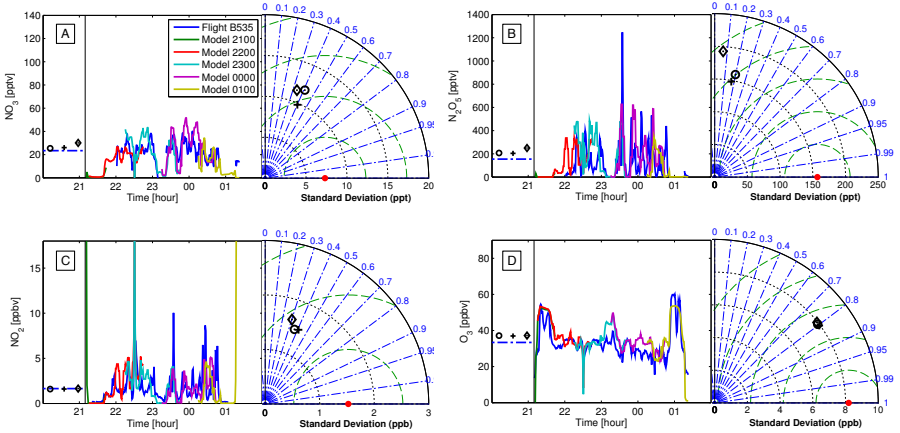

Figure 7. Flight track measurement–model comparisons for key nitrate species for flight B535. Main plots show 1 min averaged measurements (blue lines), and data from the "het on" model scenario (multi-coloured lines) for NO_3, N_2O_5, NO_2, and O_3 (**a–d**, respectively). The side panels on the left of each plot show the mean values for each diagnostic species along the flight track, while the Taylor diagrams on the right shows the standard deviations of, and correlations between, the individual model scenarios and measurements. In these side plots the measurement data is represented by the red dot and blue dash-dotted line, while the "het on", "no Cl pathway", and "het off" model scenarios are represented by the black circle, black cross, and black diamond, respectively.

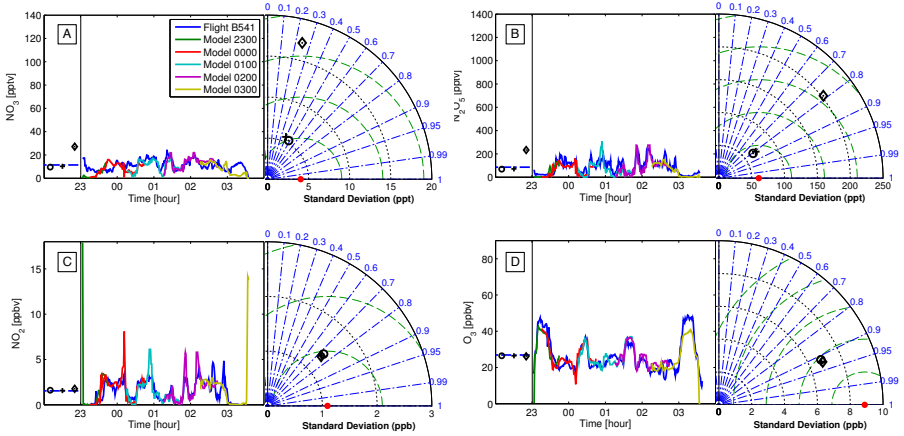

Figure 8. Flight track measurement–model comparisons for key nitrate species for flight B541. Main plots show 1 min averaged measurements (blue lines), and data from the "het on" model scenario (multi-coloured lines) for NO_3, N_2O_5, NO_2, and O_3 (**a–d**, respectively). The side panels on the left of each plot show the mean values for each diagnostic species along the flight track, while the Taylor diagrams on the right shows the standard deviations of, and correlations between, the individual model scenarios and measurements. Symbols representing the different model scenarios are the same as those used in Fig. 7.

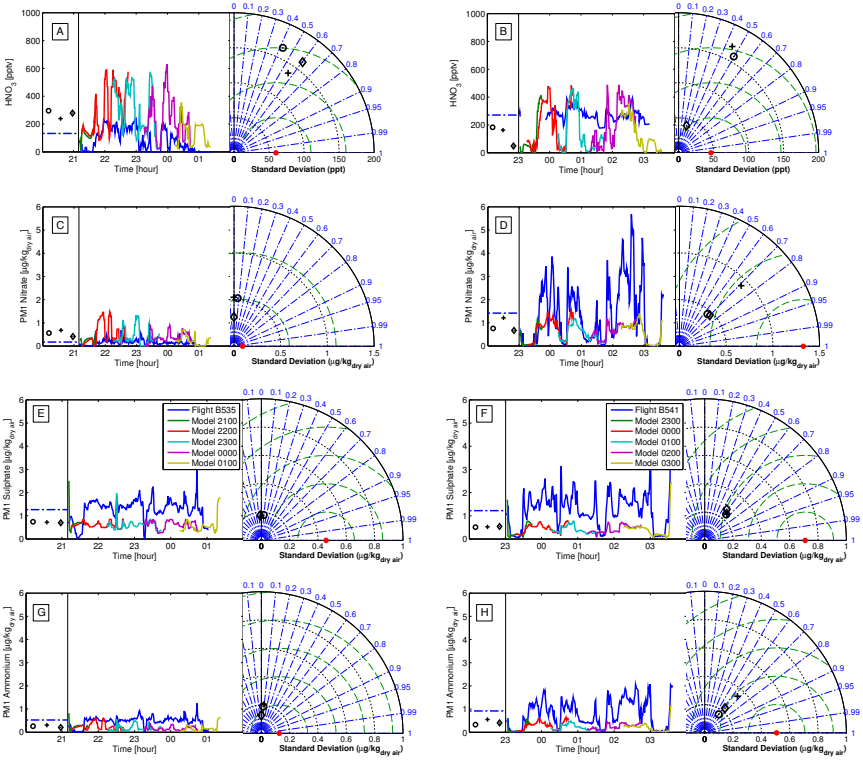

Figure 9. Flight track measurement–model comparisons and statistics for gas-phase HNO_3 and PM_1 Nitrate, Sulphate, and Ammonium for flight B535 (**a**, **c**, **e**, and **g**, respectively) and flight B541 (**b**, **d**, **f**, and **h**, respectively). Symbols representing the different model scenarios are the same as those used in Fig. 7.

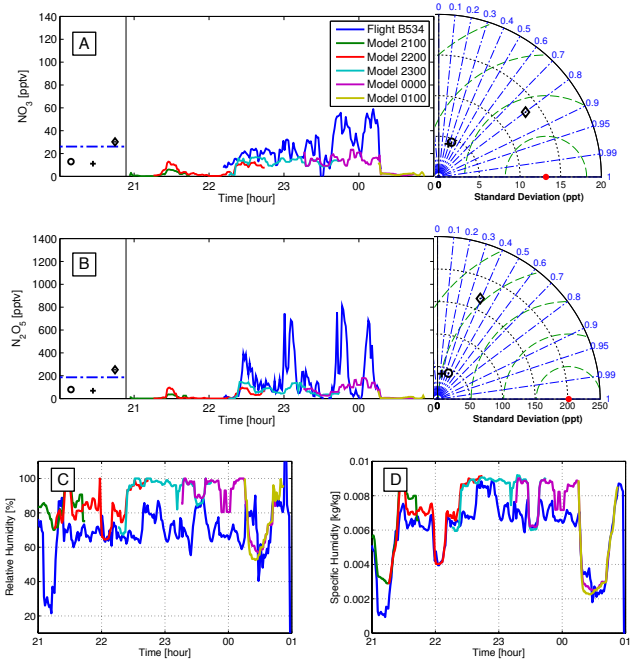

Figure 10. Flight track measurement–model comparisons and statistics for NO_3 and N_2O_5 (**a** and **b**, respectively), as well as comparisons for relative and specific humidity (**c** and **d**, respectively) for flight B534. Symbols representing the different model scenarios are the same as those used in Fig. 7.

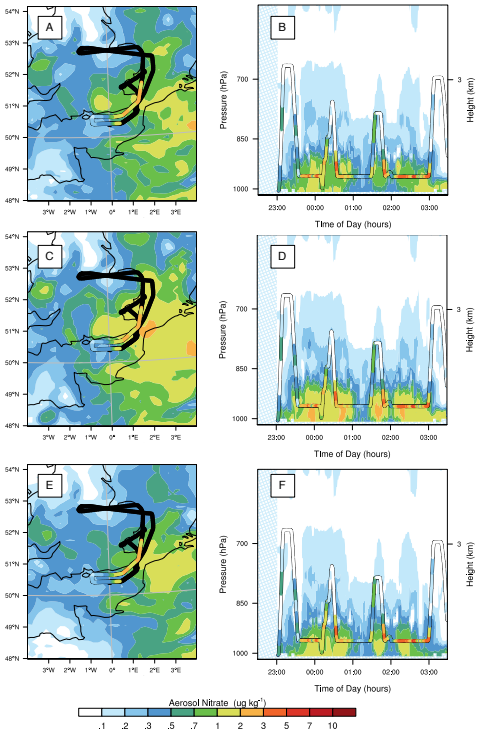

Figure 11. PM_1 nitrate mass loadings for the "het on" (**a** and **b**), "no Cl pathway" (**c** and **d**) and "het off" (**e** and **f**) for the B541 flight across the model domain. The aircraft flight track is indicated in all plots with a thick black line. Measurement data is superimposed upon that line using the same colour scale as the model data. (**a**, **c** and **e**) are horizontal slices on the 960 hPa pressure level at 01:00 UTC (incorporating measurement data between 00:30–01:30 UTC and 940–980 hPa). (**b**, **d** and **f**) are vertical curtain plots along the flight path.

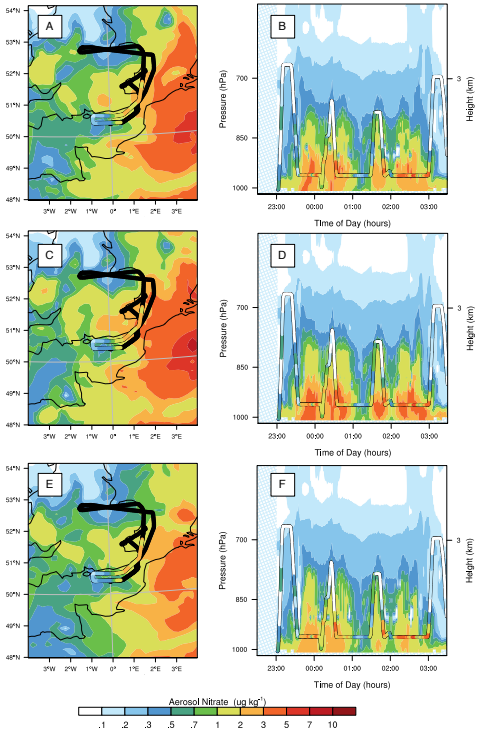

Figure 12. PM_{10} nitrate mass loadings for the "het on" (**a** and **b**), "no Cl pathway" (**c** and **d**) and "het off" (**e** and **f**) for the B541 flight across the model domain. The aircraft flight track is indicated in all plots with a thick black line. Measurement data is superimposed upon that line using the same colour scale as the model data. (**a**, **c** and **e**) are horizontal slices on the 960 hPa pressure level at 01:00 UTC (incorporating measurement data between 00:30–01:30 UTC and 940–980 hPa). (**b**, **d** and **f**) are vertical curtain plots along the flight path.

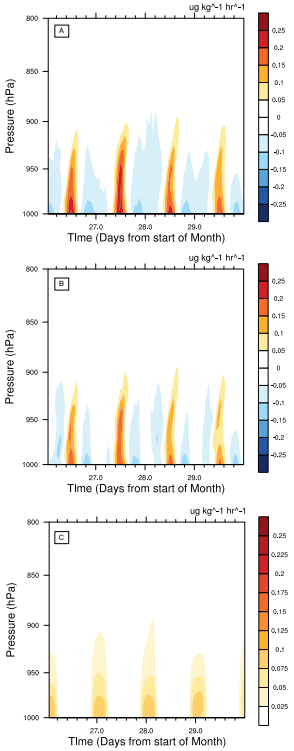

Figure 13. Domain averaged tendencies in total nitrate mass loadings. (**a** and **b**) show the incremental change in the domain mean total nitrate (aerosol nitrate plus gas-phase HNO_3) in $\mu g\, kg_{air}^{-1}\, h^{-1}$ for the "het off" and "het on" scenarios, respectively. **(c)** shows the domain mean of the integrated uptake rate of N_2O_5 (plotted as potential aerosol nitrate mass loading, without consideration of loss to the $ClNO_2$ pathway).

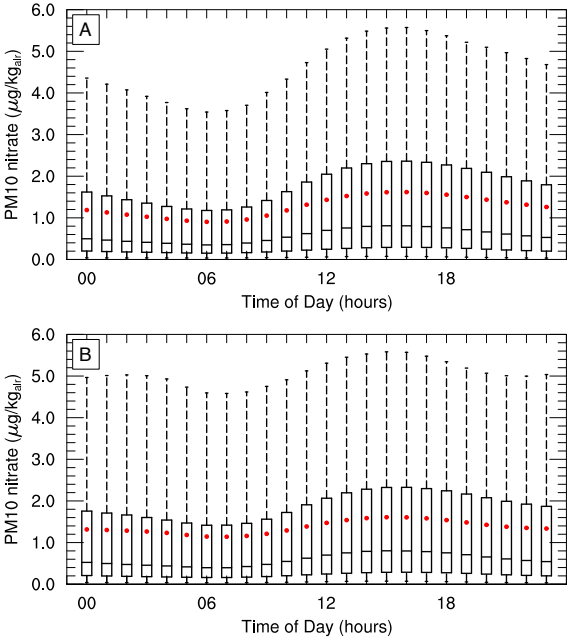

Figure 14. Statistical analysis of variation in aerosol nitrate mass loadings across the domain on the 990 hPa pressure level for the "het off" and "het on" scenarios (**a** and **b**, respectively). Hourly data from a 15 day period is used to obtain a campaign-averaged diurnal cycle (see main text for details). Whiskers indicate the 5th and 95th percentiles, while the red markers indicate mean mass loading.

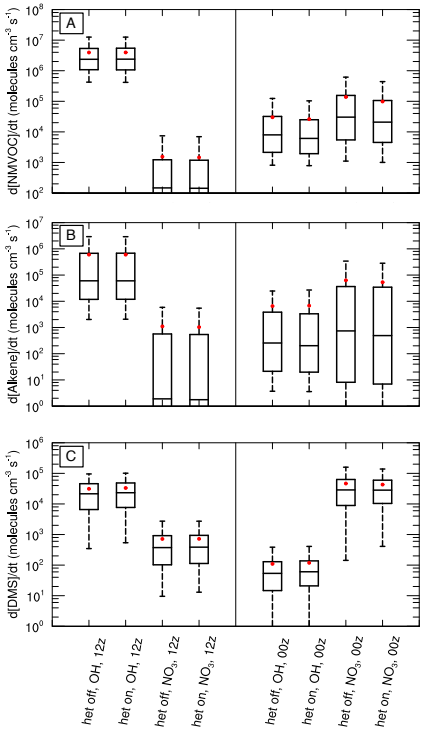

Figure 15. Statistical analysis of variation in oxidation rates, across the domain on the 990 hPa pressure level, for: total NMVOCs; Alkenes; and DMS (**a–c**, respectively). Data is presented for oxidation with respect to OH and NO_3, at midday (12:00 UTC) and midnight (00:00 UTC), and for both the "het off" and "het on" scenarios, as indicated by the x axis labels. Hourly data from a 15 day period is used to obtain a campaign-averaged diurnal cycle. Whiskers indicate the 5th and 95th percentiles, while the red markers indicate the mean oxidation rate.